Manuscript Details

Manuscript number	COST_2020_1134_R1
Title	Two-Bay Pultruded GFRP Safety Barrier/Guardrail - Testing, Analysis and Compliance with Standards
Article type	Full Length Article

Abstract

The paper describes a series of material/structural property tests on pultruded GFRP (glass fibre reinforced polymer) circular cross-section tubes used in safety barriers/guardrails. The tests enabled the elastic flexural and shear moduli of the tubes and the rotational stiffness of the post-base connections to be quantified. This information was then used to set up ANSYS FE (finite element) models of the guardrails using cubic beam elements and revolute joints to simulate the out-of-plane deflections of a two-bay plane guardrail loaded at the top of the centre-post and the mid-bays of the handrail. Load tests were carried on a full-scale guardrail in order to demonstrate that it complied with the load and deflection requirements given in the most recent design standard for guardrails. Thereafter, the ANSYS FE model deflection predictions were compared with those recorded during the load tests on the guardrail. It was shown, that including revolute joints in the model gave deflections that were, in the worst instances, within 15% of the values recorded in the physical tests.

Keywords	bending; guardrails, GFRP tubes; pultrusion; testing; torsion

Corresponding Author	Geoffrey Turvey
Corresponding Author's Institution	Lancaster University
Order of Authors	Geoffrey Turvey, Jonathan Milburn

Submission Files Included in this PDF

File Name [File Type]

Cover Letter.docx [Cover Letter]

Responses to Referee 1 and 2.docx [Response to Reviewers]

rev2 - Mauscript - text only - 14-6-20.doc [Manuscript File]

rev1 - List of Figures and Captions.doc [Figure]

rev1 - Figure 1 001.tif [Figure]

rev1 - Figure 2 001.tif [Figure]

rev1 - Figure 3 001.tif [Figure]

rev1 - Figure 4(a) 001.tif [Figure]

rev1 - Figure 4(b) 001.tif [Figure]

rev1 - Figure 5 001.tif [Figure]

rev1 - Figure 6 001.tif [Figure]

rev1 - Figure 7 001.tif [Figure]

rev1 - Figure 8 001.tif [Figure]

rev1 - Figure 9 001.tif [Figure]

rev1 - Figure 10 001.tif [Figure]

rev1 - Figure 11(a) 002.tif [Figure]

rev1 - Figure 11(b) 001.tif [Figure]

rev1 - Figure 12 001.tif [Figure]

rev1 - Figure 13 001.tif [Figure]

rev1 - Figure 14 001.tif [Figure]

rev1 - Figure 15 001.tif [Figure]

rev1 - Figure 16 001.tif [Figure]

rev1 - Figure 17 001.tif [Figure]

rev1 - Figure 18 001.tif [Figure]

rev1 - Figure 19 001.tif [Figure]

rev1 - Figure 20 001.tif [Figure]

rev1 Figure 21(a) 001.tif [Figure]

rev1 - Figure 21(b) 001.tif [Figure]

rev1 - List of Tables and Titles.doc [Table]

Table 1.doc [Table]

Table 2.doc [Table]

Table 3.doc [Table]

Table 4.doc [Table]

Table 5.doc [Table]

Table 6.doc [Table]

Table 7.doc [Table]

Table 8.doc [Table]

Table 9.doc [Table]

Table 10.doc [Table]

Conflict of Interests Form.docx [Conflict of Interest]

declaration of competing interests (1).docx [Author Statement]

To view all the submission files, including those not included in the PDF, click on the manuscript title on your EVISE Homepage, then click 'Download zip file'.

Engineering Department,
Lancaster University,
Gillow Avenue,
Bailrigg,
Lancaster,
LA1 4YW.

14th June 2020.

Professor A.J. Ferreira,
Editor,
Composite Structures,
Department of Engineering,
University of Porto,
Porto,
PORTUGAL.

Dear Professor Ferreira,

Title: Two-Bay Pultruded GFRP Safety Barrier/Guardrail – Testing, Analysis and Compliance with Standards

Authors: G.J. Turvey and J. Milburn

Please would you kindly arrange for our *revised* manuscript, referred to above, to be considered for possible publication in your journal, *Composite Structures*.

We look forward to receiving your decision on our manuscript's acceptability (or otherwise) for publication in *Composite Structures* in due course.

Yours sincerely,

G.J. Turvey

Referee 1

The Referee appears to believe the guardrail test data used in the paper was that reported in the first Author's paper ([7] in the revised, [3] in the original paper), which was published in 2015. As a result, the Referee feels that the experimental contribution is limited, because it only deals with three-point bending and torsion tests of the guardrail tubes and cantilever tests of the tube plus base to determine the rotational stiffness of the post bases. The Referee also feels that the FE analyses of the guardrails are straightforward and they do not model failure response.

Clearly, the Referee has not read [3]. The tests on the guardrails reported in [3] were carried out on a modular guardrail cantilevered from a vertical foundation, so that it could be subjected to vertical loading by means of steel weights hung from the top rail. The test results reported in [3] were not used in the present paper, because compliance of the guardrail tests with the more recent standard ([12] in the revised paper; [6] in the original paper) requires the guardrail to be in the vertical plane and the loads to be applied horizontally and normal to the vertical plane at the tops of the posts and the mid-spans of the handrail. This is pointed out in Section 5 (now Section 8 of the revised paper) of the originally submitted paper. Consequently, the guardrail tests and test data reported in the revised paper are ***new***!

The numerical models used to simulate the data obtained from the guardrail tests, may not be highly sophisticated. Nevertheless, the use of semi-rigid joint stiffnesses and linear analysis are shown to produce deflections closer to the test values than the rigid joint analysis and the differences between the analysis models and the test data have been quantified. Moreover, it appears that these are the *first* FE analyses of modular guardrails. Therefore, it is the Authors' view that these analyses represent a *new* contribution to knowledge.

The Referee appears to be critical of the fact that the failure response of the guardrail and the post bases have not been considered. No such failures were observed! The guardrail was able to sustain the strength loads specified in the standard ([12) in the revised paper; [6] in the original paper) without damage. It is, perhaps, unfortunate that in [6] the maximum load that has to be applied in a modular guardrail test is referred to as the *strength* load. Most engineers associate this terminology with *failure*!

The first Author wishes to point out that further load tests on guardrails have been carried out at higher loads and failures in bases and joints have been observed. However, it was never the intention to report these tests in the present paper. Both Authors believe that the test work and the numerical simulations presented provide *new* and *useful* contributions to knowledge.

Referee 2

The Authors do not agree with the first sentence of the Referee's opening paragraph. They have demonstrated that linear FE analysis with semi-rigid joints is able to predict the deflections of the guardrail with reasonably good accuracy, when tested in accordance with the BS standard ([12] in the revised paper; [6] in the original paper). Furthermore, it has been demonstrated that the guardrail is able to support the *so-called* strength load without sustaining any damage or exceeding the deflection limits (maximum and residual)!

The Authors' responses to the detailed criticisms 1 – 19 are as follows:-

1 Yes, the lower self-weight of pultruded GFRP guardrails compared to steel guardrails is beneficial in general, because large pre-assembled sections of multi-bay guardrails can be lifted manually. Lower self-weight also means that transportation costs to site are cheaper. The use of lighter guardrails on offshore platforms is beneficial. It is often said that each unit of topside mass saved, saves nine units of sub-surface mass. There are many other benefits compared to steel: GFRP has high corrosion resistance and good thermal and electrical insulation properties.

2 This statement has been removed in the light of the additional references noted under Item 19.

3 This statement has been removed.

4a Figures 1, 19 and 20 have been replaced by Figure 19 with minor additions (now Figure 1), thereby *reducing* the number of figures by two.

4b Figure 3 has been deleted.

4c Figures 6 and 7 has been deleted.

5 It is pointed out that the elastic and shear moduli given in Tables 2 and 4, respectively are used in the simple hand calculations. The calculations have been re-done and the percentages due to shear deformation have been amended.

6 The Authors believe that their value for the shear modulus is reasonable, as they have conducted torsion tests on many of these tubes in other projects and have obtained values from about 2.5 to 3 GPa. As of now they have not been able to use micro-mechanical modelling to calculate the value of the shear modulus, because they do not know the details of the lay-ups (fibre volume fractions, particular types of glass fibre and polyester resin) used in the tubes.

The Authors do not believe that the adhesive bond between the plugs and the tube has any significant effect on the shear modulus, not least because in the torsion tests the maximum angle of twist was small, ranging from about 2.8 to 5.2 degrees. The torsion test rig has been used a number of times by different individuals and typical shear modulus values of approximately 3 GPa have been obtained. However, the Authors do concur that by using the full expression for the polar second moment of area the calculated shear modulus may increase by around 10%.

7 The Authors have reduced the number of decimal places of the values given in these tables to two.

8 The Authors do not have any *sharper* images. However, they believe that the reader can fully understand the images, as explained in the figure caption.

9 The highlighted text has been added to the sentence.

10 The Authors accept that it would have been beneficial to have had a clinometer on the *shoe* of the post base. However, good correlation of the rotational stiffnesses, defined by the straight-line fit to the higher load test data, confirms the validity of rotational stiffnesses used at the higher test loads, which are important for the FE – test comparisons of the guardrail deflections.

11 The word *connection* has been changed to *joint*.

12 The Authors are unable to say whether or not the fit of the post in the shoe of the base was tight or with a degree of clearance.

13 The Authors believe the simple analysis becomes inaccurate at low loads, but it is more accurate at higher loads and these are the most relevant to the comparisons between the FE and test results of the guardrail.

14 The word *standard* has been substituted for the word *code*.

15 The word *weights* has been added.

16 It is explained that there are always practical variations within any structure, which mean it will not exhibit perfectly symmetric or antisymmetric deformations in response to such load conditions.

17 The word *reliable* has been substituted for *accurate*.

18 The Authors have saved a lot of space by reducing the total numbers of figures from 27 to 21. However, they have decided to retain the original format of Table 10. Even though, it is a little larger (in terms of space

occupied on the page) than the Referee's table Moreover, there is no need to be repeatedly referring to the three footnotes to the Referee's table.

19 The two additional references have been added to the literature review in the Introduction. In addition, the Authors have referred to several relevant Lancaster University Engineering Department reports on guardrail and post tests, which have supported the UK's pultrusion industry during the past three decades.

Conclusion

The Authors believe that they have addressed the Referees' comments/criticisms to the best of their ability and are hopeful that the Referees will now recommend their paper for publication in *Composite Structures*.

Two-Bay Pultruded GFRP Safety Barrier/Guardrail – Testing, Analysis and Compliance with Standards

by

G.J. Turvey[a] and J. Milburn[a,b]

[a]Engineering Department, Lancaster University, Bailrigg, Lancaster, LA1 4YW, UK

[b]Cygnet Texkimp, Swan House, Kimpton Drive, Wincham Lane, Northwich, CW9 6GG, UK

Abstract

The paper describes a series of material/structural property tests on pultruded GFRP (glass fibre reinforced polymer) circular cross-section tubes used in guardrails. The tests enabled the elastic flexural and shear moduli of the tubes and the rotational stiffness of the post-base connections to be quantified. This information was then used to set up ANSYS FE (finite element) models of the guardrails using cubic beam elements and revolute joints to simulate the out-of-plane deflections of a two-bay plane guardrail loaded at the top of the centre-post and the mid-bays of the handrail. Load tests were carried on a full-scale guardrail in order to demonstrate that it complied with the load and deflection requirements given in the most recent design standard for guardrails. Thereafter, the ANSYS FE model deflection predictions were compared with those recorded during the load tests on the guardrail. It was shown, that including revolute joints in the model gave deflections that were, in the worst instances, within 15% of the values recorded in the physical tests.

1. Introduction

Safety barriers, also referred to as guardrails, are one of the most common types of secondary structure in the world. Many centuries ago they were made from rough-hewn timber which nowadays would be referred to as fencing. During the past two hundred years cast/wrought iron and mild steel have been used to form the posts and rails of guardrails. However, without the use of protective measures, such as surface coatings etc., these guardrails start to degrade relatively rapidly, especially in marine environments. Other more expensive materials such as aluminium and stainless steel are used in guardrails, especially where corrosion resistance/durability is important.

However, during the past three decades glass fibre reinforced polymer (GFRP) composite tubular profiles manufactured by the pultrusion process [1] have begun to be used in safety barriers. The particular advantages driving these changes are the profiles' lower self-weight and higher resistance to adverse environmental conditions than their metallic counterparts. The former characteristic, together with simple molded two-part multi-way mechanically fastened joints, facilitates manual on-site assembly and reduces transportation costs, whereas the latter characteristic reduces maintenance costs. Both low self-weight and resistance to adverse environmental conditions are particularly important for offshore structures, where it is said that each unit of topside mass saved, saves nine units of sub-surface mass and the high resistance of GFRP to seawater conditions is clearly advantageous.

Since the early 1990s the first author and his collaborators have assisted the UK's pultrusion industry in undertaking a number of experimental investigations to confirm the utility of pultruded GFRP modular and heavy duty guardrails and their components [2 – 6], which are used to protect pedestrians and construction site workers from falling off walkways, floors under construction, raised platforms etc. In more recent times, some of these research investigations have started to be published [7] along with those of other researchers, who have investigated experimentally pultruded GFRP guardrails of a similar overall size, but using corrugated rather than smooth surface tubes and multi-way joints which are inserted into the ends of the tubes [8 & 9].

Although not strictly relevant to the present paper, it should be mentioned that other forms of pultruded GFRP guardrails have been the focus of research, namely very heavy duty guardrails (often referred to as *crash barriers*) which serve to restrain vehicles from exiting the highway during crashes. These very heavy duty guardrails are different in both form and make-up from those under consideration in the present paper and, therefore, will not be considered further. However, the interested reader may refer to [10] for further details.

It should be appreciated that none of the lightweight modular guardrails in [7 – 9] deal with analysis/numerical modelling of guardrails and, therefore, do not assess how well they are able to predict the load – deformation

characteristics of the guardrails observed during tests. In addition to addressing the accuracy of numerical modelling in predicting the load – deformation response of lightweight guardrails, the paper also establishes whether or not the guardrails considered herein comply with the more recent UK test standards [11 & 12].

The pultruded GFRP modular guardrail, described herein, is referred to as a plane two-bay guardrail (see Figure 1). The GFRP tubes forming the vertical posts and horizontal rails have smooth surfaces, are circular in cross-section with outside diameters of 50 mm and wall thicknesses of 5 mm. The upper and lower rails are referred to as *hand* and *knee* rails, respectively. The three post bases are identical and each post is joined to its base by a single bolt and four bolts join the base to the foundation. Three types of two-part connector are used to join the posts to the rails. Two two-way connectors join the ends of the hand rail to the tops of the outer posts and a three-way connector joins the hand rail to the top of the interior post. In addition, two three-way connectors join the outer ends of the single-bay knee rails to the mid-height of the outer posts and a single four-way connector joins the inner ends of the knee rails to the mid-height of the interior post. The overall dimensions of the guardrail are also shown in Figure 1, which are in compliance with the standards [11 & 12].

2. Geometric Properties of the Pultruded GFRP Tubes

In order to be able to set up Finite Element (FE) models of the modular guardrail it was first necessary to determine the geometric properties of the pultruded GFRP tubes. Hence, two tubes (I & II) were selected for this purpose. Four lines, labelled A, B, C and D (see Figure 2) were drawn along the surface of each tube parallel to its axis. The lines were spaced at 90^{o} intervals around the circumference.

The outer and inner diameters and wall thicknesses were measured at locations A – D around both ends of the tubes. The mean values, standard deviations and coefficients of variation of these measurements are given in Table 1.

3. Elastic Flexural Moduli of the Pultruded GFRP Tubes

Three-point bending tests were used to determine the flexural moduli of the tubes I and II. Therefore, 50 mm in from each end of the tubes I and II circular lines were drawn around the circumference to mark the positions of the simple supports and to define their respective spans of 1 and 1.2 m. These lines helped with the alignment of the tubes on their supports.

In a three-point flexure test the mid-span deflection is influenced by the tube's material properties, i.e. its elastic flexural and transverse shear moduli. However, the effect of the transverse shear modulus reduces as the tube's span to depth ratio increases. Simple hand calculations, based on the mean flexural elastic and shear moduli (see Tables 2 and 4), show that for tube spans of 0.5, 1 and 1.5m the effect of shear on the mid-span deflection is 15.8, 4 and 1.8% respectively. Therefore, it was decided to carry out three-point flexure tests on two tubes with spans of 1 and 1.2 m respectively to determine their flexural moduli.

Each beam was tested by adding 10 kg slotted steel disk masses to a 1 kg steel load hanger at mid-span until the maximum load of approximately 991 N was reached. The tube was then unloaded. After each load increment/decrement was applied/removed the tube's mid-span deflection was recorded using a dial gauge in contact with the top surface of the load hanger collar (see Figure 3). The dial gauge had a maximum travel of 50 mm and an accuracy of 0.01 mm. The two tubes were subjected to three load – unload tests for each orientation, i.e. with lines A – D uppermost in turn, so that a total of twenty-four tests were carried out, i.e. 12 on each tube. The maximum mid-span deflections recorded for the 1 m and 1.2 m spans ranged from 3.32 to 3.60 mm and 5.79 to 6.09 mm, respectively.

From the load and deflection data obtained for each tube orientation, load versus mean mid-span deflection plots were constructed. Examples of these are shown in Figure 4 for the 1 m and 1.2 m spans, loaded with Lines A and C uppermost, respectively.

From Figure 4 it is self-evident that the load versus mean mid-span deflection response is linear. This characteristic may be used to determine the flexural moduli of the tubes. The equation for the mid-span deflection of a uniform cross-section simply supported tube subjected to three-point flexure is:-

$$\delta_C = \frac{WL^3}{48EI} \tag{1}$$

In Eq.(1) δ_C is the mid-span deflection, W is the load applied at mid-span, L is the tube span, E is its flexural elastic modulus and I is its second moment of area, which is the same for all axes of flexure for a truly circular cross-section tube.

Eq.(1) may be expressed explicitly in terms of the flexural elastic modulus as:-

$$E = \frac{L^3}{48I}\left(\frac{W}{\delta_C}\right) \tag{2}$$

The bracketed quotient on the right hand side of Eq.(2) represents the slope of the load versus mean mid-span deflection data. Hence, by determining the slopes for each of the test orientations (A – D) of the 1 and 1.2 m span tubes, eight values of the flexural elastic modulus can be calculated. These are given in Table 2 together with the overall mean and standard deviation.

4 Shear Moduli of the Pultruded GFRP Tubes

In order to obtain the shear modulus of the pultruded GFRP tubular material, it was decided to carry out uniform axial torsion tests on three lengths of tube. If the tube is assumed *thin-walled*, then the shear stress at each end may be expressed as:-

$$\tau = \frac{T}{2\pi r^2 t} \tag{3}$$

In Eq.(3) r is the tube's mean radius and t is its wall thickness. The shear modulus G may expressed as:-

$$G = \frac{\tau}{\gamma} \tag{4}$$

In Eq.(4) τ and γ denote the shear stress and shear strain, respectively, in the tube wall.

In order to carry out the required axial torsion tests to determine the shear moduli of the GFRP tubes, it is necessary to have some means of applying equal and opposite torques at opposite ends of the tube. This was achieved by means of two bonded-in steel plugs. A longitudinal cross-section of a tube with a plug at each end is shown in Figure 5.

In order to record the outer surface strains during the torsion test a pair of biaxial strain gauges were bonded to the tube's surface at mid-span on axial lines 180° apart. The sensitive axes of the gauges were oriented at +/- 45° to the axial lines, as shown in Figure 6. Each gauge was 5 mm long with an internal resistance of 120 Ohms.

The strains recorded on the outer surface of the tube (induced by the equal and opposite end torques T) enable the shear strain γ to be calculated as follows:-

$$\gamma = \frac{\varepsilon_1^{+45^o} + \varepsilon_2^{+45^o}}{2} - \frac{\varepsilon_1^{-45^o} + \varepsilon_2^{-45^o}}{2} \tag{5}$$

In Eq.(5) the strains $\varepsilon_1^{+45^o}$ and $\varepsilon_2^{+45^o}$ denote the direct strains measured by the two gauges oriented at $+45^o$ to the tube's axis. Likewise, the strains $\varepsilon_1^{-45^o}$ and $\varepsilon_2^{-45^o}$ are the strains recorded by the gauges at -45^o to the axis.

The torsion tests were carried out on the same tube. The overall length of the tube in the first test was 570 mm, i.e. a 500 mm torsion span plus 35 mm at each end to accommodate the bonded steel plugs. After completing the first torsion test, the tube was removed from the test rig and its overall length was reduced to 470 mm. The two plugs were removed from the tube offcuts and then cleaned. They were then bonded into the ends of the tube to give a torsion span of 400 mm. The third and final torsion test was carried out for an overall length of 370 mm, giving a torsion span of 300 mm. A tube set up ready for testing is shown in Figure 7.

The instrumentation on the torsion rig included an 800N capacity load cell connected to a 125 mm lever arm at one end of the rig. A spirit level was positioned along the lever arm and was used to check that the arm was horizontal and the load cell was vertical prior to logging the end torque. At the other end of the test rig a torque wheel was used to apply the twist to the adjacent end of the tube. Connected to the other end of the torque wheel's spindle was a graduated disk which measured the rotation of the tube due to the applied torque.

Prior to setting up each tube in the torsion test rig its outer and inner diameters and wall thicknesses were measured at four locations – two at each end at opposite ends of a diameter. These dimensions together with their means, standard deviations and coefficients of variation are given Table 3.

The test procedure was straightforward. Once the tube had been positioned in the test rig, the sprit level was checked and, if necessary, adjusted to ensure that the lever arm connected to the load cell was horizontal. Thereafter, the initial torque and rotation readings were noted. A load increment of 50N was then applied by rotating the torque wheel and the angle of rotation was noted before and after levelling the spirit level. The strain readings were also noted. The procedure was then repeated successively until the load measured 400 N. Thereafter the tube was unloaded in 50 N decrements to zero load.

After checking the data obtained for each torsion test, the shear stresses and strains were calculated using Eqs. (3) and (5) and shear stress versus shear strain graphs were plotted. An example is shown in Figure 8 of the graph for the 400 mm long tube.

As is evident from Figure 8, the loading part of the shear stress versus shear strain response is sufficiently linear, so that Eq.(4) can be used to determine the shear modulus for each tube length. The results of these calculations are shown in Table 4.

5 Tests to Determine the Rotational Stiffness of Post Base Joint

The most significant loads that guardrails have to resist are horizontal loads on the top rail directed normal to the vertical plane of the guardrail. These loads produce significant bending of the vertical posts, which has to be resisted by the joints at their bases. Hence, it is especially important to be able to quantify the rotational stiffness of the post-base joints, if FE models are used to analyse and design guardrails.

Figure 9 shows dimensioned plan and elevation drawings of the post bases used in the two-bay guardrail shown in Figure 1. An isometric drawing is also shown in Figure 9 in order to give an overall view of the base. The *foot* of the post slots into the the vertical short cylinder (sometimes referred to as the *shoe*) and is fastened to it by a single bolt. The square flat part of the base (its *sole*) is connected to the guardrail's foundation by four bolts. There are four *stub* stiffeners together with a transition zone between the base of the shoe and the top surface of the sole which enhance the rotational stiffness of the post-base joint.

In order to be able to quantify the rotational stiffness of the post-base joint, the assembled post and base may be conveniently idealised as a simple tip-loaded tubular cantilever with a semi-rigid (rather than the usual rigid) joint at its support. This simple idealization is illustrated in Figure 10.

Assuming that the flexural elastic modulus of the tube is E, its second moment of area is I, its length is L, its rotational stiffness at support A is K, and a vertical load W acts at its free end B, then the deflection δ_B may be expressed as:-

$$\delta_B = \frac{WL^3}{3EI} + \frac{WL}{GA} + \frac{WL^2}{K} \tag{6}$$

In Eq.(6) the three terms on the right hand side of the equation are the bending, shear and joint stiffness contributions to the tip deflection.

Eq. (6) may be re-arranged to give the rotational stiffness as:-

$$K = \frac{WL^2}{\left(\delta_B - \frac{WL^3}{3EI} \left\{ 1 + \frac{3EI}{GAL^2} \right\} \right)} \tag{7}$$

From Eq.(7) it is self-evident that by carrying out load tests on tubes set up as cantilevers (see Figure 10), the rotational stiffness K of the post base may be evaluated. However, before carrying out such a test, it is important to realise that the post may be joined to the base with the bolt holding the post in place in one of two possible orientations (see Figure 11).

Intuition suggests that the bolt orientation parallel to the plane of flexure, as depicted in Figure 11(b), is likely to result in a stiffer guardrail. In order to verify this, one end of the two tubes was connected to a post base. In one of the bases the bolt was normal to the plane of flexure and in the other it was parallel to the plane. Each post-base was then bolted to a rigid support to create a 900 mm long tubular cantilever. Thereafter the cantilever was loaded incrementally up to a maximum load of 147.15 N and then unloaded to zero load. Tip deflections were recorded for each load increment/decrement. This load – unload procedure was repeated three times for each cantilever. The mean tip deflections at the maximum load for the bolts parallel and normal to the plane of flexure were 7.19 mm and 8.60 mm, respectively. These results confirmed the original expectation.

Based on these findings, it was decided to test another cantilevered tube with the bolt in the shoe parallel to the plane of flexure. Prior to setting up the tube for the cantilever tests the cross-section dimensions were measured at both ends. The measured dimensions are given in Table 5.

Figure 12 shows the setup for the cantilever tests. In the first test the load was applied at 1100 mm from the base of the post and in the second test at 800 mm from it. In both tests the deflections and rotations were recorded for each load increment/decrement. Each test was repeated three times with Line A uppermost and three times with Line C uppermost.

The moment versus semi-rigid support rotation data obtained from the tests appear to be reasonably linear over most of the range, though the very low load rotation data was difficult to obtain. However, most of the moment and rotation data appear to exhibit reasonably good linear correlations at the higher loads, which are of most interest for the FE analyses presented later in the paper. The straight line fits to the test data (see Figure 13) have been used to obtain joint rotational stiffnesses of 114 and 118 kNm/rad for the two cantilever tests. Hence, a mean rotational stiffness of 116 kNm/rad is assumed for the post-base when the bolt connection is parallel to the plane of deformation.

6. ANSYS Models of the Cantilever Beam Tests

Before starting to set up Finite Element (FE) models of the guardrail tests, it was deemed sensible to set up a model of the cantilever beam test with a semi-rigid support in order to check how well its rotational spring stiffness was able to predict the test results.

Figure 14 is a physical illustration of a revolute joint between two members (red and blue) which can rotate about a common axis normal to the plane of the members. In the FE model of the tip loaded cantilever tests, the semi-rigid joint at the support is represented by a revolute joint element. The joint is a two-node element of zero length. The left hand node is connected to right hand node of the foundation element and the other to the left hand node of the cantilever element (see Figure 15). The right hand node of the cantilever element is subjected to the vertical tip load. The rotational stiffness of the cantilever's semi-rigid joint (the revolute joint) is assumed equal to the mean of the two rotational stiffnesses measured in the 800 and 1100 mm tip-loaded cantilever tests, i.e. 116 kNm/rad.

It is evident from the results in Table 6 that the mean deflections obtained from the ANSYS FE model are on average 11% greater than the corresponding experimental values. However, this difference reduces somewhat at the higher loads. Furthermore, the accuracy of the loading point rotation obtained from the ANSYS FE analysis is only about 2.5% higher than the measured values. Based on these results correlations it was decided that the rotational stiffness of the semi-rigid joint could be used in the subsequent FE analyses of the two-bay guardrails,

especially as it was impractical to conduct separate tests to try to determine the semi-rigid rotational stiffness of each two-part multi-way joint.

7. ANSYS FE Models and Analysis of Two-Bay Guardrails

The overall dimensions of the two-bay guardrail are shown in Figure 1. These dimensions were chosen to comply with two relevant UK design standards, namely BS 4592-0 [11] and BS EN ISO 144122-3 [12]. These criteria are:-

1. A two-bay guardrail must be tested.

2. The distance between the top of the guardrail (the handrail) and the foundation must be at least 1100 mm.

3. The distance between the top (hand) rail and the lower (knee) rail must not be greater than 500 mm.

4. The distance between post (stanchion) axes must not be greater than 1500 mm.

5. The guardrail must be bolted *upright* to a rigid foundation and the individual test loads must be applied *normal* to the vertical plane at the tops of the posts and the mid-spans of the handrails.

In Figure 1 the posts are shown joined to their respective bases by single bolts through their shoes parallel to the plane of flexure, so that the higher semi-rigid rotational stiffnesses obtained from the cantilever tests may be used in the ANSYS FE analysis models.

Figure 1 shows the guardrail with the loading positions on the three posts labeled A, C and E and the mid-spans of the hand rail labelled B and D. The loads, which are applied in separate tests act normal to the plane of the guardrail. They are defined in [12]. For the present guardrail analyses only the maximum load will be considered, i.e. 697 N. This is 41 N greater than the value specified in [12], because the loads used in the tests were in the form of slotted steel disk weights. Furthermore, according to [12] one test must be carried out with the load applied at C and another with the load at the mid-span B or D.

Three ANSYS FE models of the guardrail were set up for analysis with Nodes A – E, as shown in Figure 16. Each model used two-node cubic beam elements to represent the posts and rails. However, because the loads at Nodes B and D were at the mid-bay positions on the handrail, they were modelled with two beam elements. The principal differences between the three FE models, Models 1 – 3, are the representation of the joints between posts and rails and the posts and bases, as set out below:-

Model 1: In this model all of the guardrail joints are rigid joints.

Model 2: In this model all of the joints, except the three post-base joints are rigid joints. The post-base joints are modelled as revolute joints, as described above, with a rotational stiffnesess of 116 kNm/rad.

Model 3: In this model resolute joints, with the aforementioned rotational stiffness, are used for all of the guardrails joints, except at the mid-span of the handrail (see Figure 16),

Models 1 – 3 were first analysed with the maximum load of 697 N applied normal to the plane of the guardrail at Node C. The deflection results for Nodes A – E are presented for each model in Table 7. Subsequently, the three guardrail models were re-analysed with the maximum load applied at Node B. The nodal deflections obtained for this case are also given in Table 7.

It is evident that when the load is applied at Node C the maximum difference between corresponding nodes of Models 1 and 2 range from approximately 10 – 17%. However, the differences between the deflections of Models 2 and 3 are negligible. On the other hand, when the load is applied at Node B the percentage differences between the Model 1 and 2 deflections range from about 5 – 14% and again, the differences between the Model 2 and 3 deflections are negligible.

8. Load Testing of a Modular Guardrail

In [7] the first author reported on load tests carried out on a modular guardrail to check its compliance with the requirements specified in [11]. In these tests the guardrail was cantilevered from a vertical framework. The advantage of this arrangement was that the loads could be applied by slotted steel disk weights on load hangers. However, for the present tests, it was decided to undertake load tests which met the compliance requirements specified in [12]. According to this standard a two-bay guardrail has to be fabricated and set up in a vertical plane and the loads have to be applied horizontally and normal to the vertical plane at the top of the interior post and at the mid-spans of the handrail. Therefore, it was decided to fabricate and set up a guardrail with the overall dimensions as shown in Figure 1. An image of the guardrail with its post bases bolted to a rigid channel section of steel meccano, which is bolted to the laboratory strong floor, is shown in Figure 17.

According [12] three separate load tests have to be carried out on the guardrail in order to check its compliance with the standard's requirements. These loads vary according to the post spacing, which must not exceed 1.5 m. The post spacing of the guardrail in Figure 17 is 1.25 m (see also Figure 1). The three load tests that the guardrail must satisfy are: (a) a pre-load test $\left(F_p\right)$, (b) a usability load test $\left(F_u\right)$ and (c) a strength load test $\left(F_s\right)$. These loads are calculated as follows:-

$$F_p = 75L \tag{8}$$

$$F_u = 300L \tag{9}$$

$$F_s = 1.75F_u \tag{10}$$

In Eqs, (8) and (9) $L = 1.25$ for the present post spacing.

However, because 20 kg slotted steel disk weights and a 1 kg load hanger were used to load the guardrail, it was not readily practical to apply the exact loads determined for Eqs.(8) – (10), especially as each test was repeated three times. Hence, slightly higher loads than the calculated values were applied. The calculated and actual loads are given in Table 8.

During each load test the loads were applied incrementally and the deflections at the specified points on the handrail (Nodes C, B or D) were recorded during both loading and unloading.

The purpose of the preload test was to eliminate the effects of *bedding in* during the usability and strength tests. After unloading, the deflection gauges were re-zeroed. The usability and strength tests were then carried out three times.

In order to be able to transmit the loads, provided by the slotted steel disk weights, horizontally and normal to the plane of the guardrail a pulley system was connected to a vertical steel meccano channel that was bolted to the strong floor, as shown in Figure 18.

The first usability and strength load tests carried out on the guardrail were with the load applied at the top of the interior post, i.e. at Node C (see Figure 16) and the deflections were recorded at Nodes A, C and E. The loading arrangement together with the dial gauge used to record the deflection and the electronic clinometer for measuring the rotation are shown in Figure 19. The dial gauge has a deflection range of 50 mm and an accuracy of 0.01 mm and electronic clinometer has an accuracy of 0.001 degrees.

The second series of guardrail tests were mid-bay tests. The first test was with the load applied at Node B. In this test the deflections were also measured at Nodes A, B, C and E.

The load versus mean deflection response of the guardrail tested at the top of the centre-post, i.e. at Node C, together with the mean deflections at Nodes A and E are shown in Figure 20. It is evident that at the usability load of 402 N, the deflection at Node C is 18.65 mm, which amounts to 62% of the maximum permitted deflection of 30 mm. As for the strength load of 697 N, the deflection at Node C is 31.68 mm, i.e. only about 5.6% above the usability limit deflection. Figure 20 also reveals that the mean deflections at the tops of the end posts, i.e. Nodes A and E, are not equal with the deflection at Node E being somewhat greater than that at Node A. Hence, the guardrail is not behaving entirely symmetrically (as predicted by the ANSYS FE analysis).

The load versus mean mid-bay deflection tests are shown in Figure 21, i.e. part (a) for the load at Node B and part (b) for the load at Node D. It is evident that, in both cases, the maximum deflection arises at the loaded

node. The mean deflection at Node B is 35.56 mm and that at Node D is 36.84, so that the latter deflection is about 3.6% greater than the former deflection. Moreover, the guardrail deflections for the loads at Nodes B and D are not antisymmetric reflections of each other, as they are in the ANSYS FE models. Moreover, no failure of the guardrail was detected at the maximum load of 697 N.

From the usability test data with the loads applied at Nodes B and D, respectively, it was observed that in the former case the mean deflection was 20.32 mm and in the latter case it was 22.21 mm, so that the latter deflection was about 9% greater than the former deflection. However, in both cases these deflections were significantly less than the maximum permitted deflection of 30 mm.

After unloading the guardrails loaded at Nodes A, B and D, respectively it was found that the largest residual deflection was at Node A when the load was applied at Node B. Its value was 1.36 mm which amounts to about 36% of the maximum permitted value of 3.75 mm. Hence, the guardrail passed all of the test criteria specified in [12].

9. Comparison of the Nodal Deflections of the ANSYS FE Models with the Experimental Deflections

The comparisons of the nodal deflections determined for the three FE models and the experimental tests for centre-post loading of 697N are presented in Table 9.

The results in Table 9 show that Models 2 and 3 give reasonably accurate predictions of the test deflections at Node A and Node C, where the load is applied, but underestimate the deflection at Node E by about 15%. Furthermore, the experimental deflections are not quite symmetric with respect to Node C.

A further comparison of the nodal deflections determined for the three FE models and the experimental tests for the mid-bay loading cases are shown in Table 10.

It is evident from Table 10 that when the mid-bay load is applied at Node B Model 3 under-estimates the deflections at Nodes A, B and C by 13 - 15% and over-estimates the deflection at Node E by about 6%. Likewise, when the load is applied at Node D, Model 3 under-estimates the deflections at Nodes C, D and E by 16 – 20% and over-estimates the deflection at Node A by about 3%. Furthermore, the two sets of experimental results are not quite antisymmetric with respect to Node C.

10. Concluding Remarks

The centre-post and mid-bay load tests showed that the two-bay guardrail was able to sustain the pre-load, as well as the usability and strength loads without violating the maximum and residual deflection criteria defined in [12]. Moreover, there was no evidence of any damage to the guardrail's joints.

It is also evident that the ANSYS FE Model 2 and 3 analyses (incorporating revolute joints) of the centre-post and mid-bay load tests on the guardrail were more accurate than the Model 1 analysis with rigid joints. The nodal deflections of Model 1 were all lower, sometimes up to 25 – 29%, than the corresponding experimental values.

The one-dimensional linear FE analyses presented may be relatively simple, nevertheless, as far as the Authors are aware, they are the first to be applied to lightweight modular guardrails. It appears that hitherto only experimental tests have been published (see [7] – [9]). And, moreover, it has been shown that the use of revolute joints with stiffnesses obtained from cantilever load tests increase the accuracy of the FE modelling.

Finally, it should be pointed out that, unlike the guardrail tests reported in [7] which were conducted with the guardrail in the horizontal plane and the dead-weight loading in the vertical plane, the tests reported herein were carried out with guardrail upright and the loads applied horizontally and normal to the plane of the guardrail, i.e. in compliance with the standard. Moreover, the maximum and residual deflections of the handrail of the guardrail satisfied the standard's requirements without any damage being evident in the post bases and the joints between the posts and the rails.

11. Acknowledgements

The Authors wish to record their appreciation to the Engineering Department for access to and the use of its material and structural testing facilities and to the department's technician staff for help and advice in carrying out the test work.

12. References

1.Anon., EXTREN Design Manual, Strongwell, Bristol Virginia, USA, 1989.
2.Slater RC and Turvey GJ. Tests on GRP posts and handrailing system, Lancaster University Engineering Department Report; April 1991.
3.Turvey GJ and Slater RC. Tests on pultruded GRP posts for handrail/barrier structures. *1st International Conference on Advanced Composite Materials in Bridges and Structures*, Sherbrooke, 7th-9th October 1992. Published in *Advanced Composite Materials in Bridges and Structures*, Edited by K.W. Neale and P. Labossiere, Canadian Society for Civil Engineering, (1992), 319-329.
4.Turvey GJ. Report on pultruded GRP post and handrail tests, Lancaster University Engineering Department Report; July 2003.
5.Turvey GJ and Salisbury M. Tests on pultruded post and rail safety barriers, Lancaster University Engineering Department Report LU02011, 10th October 2012.
6.Turvey G.J. An experimental investigation of the serviceability, ultimate and failure loads of pultruded GFRP tubular posts with bolted composite bases, Lancaster University Engineering Department Report No.2018-1, November 2018, pp.13
7.Turvey G.J., Experimental investigation of the load-deformation behaviour of pultruded GFRP modular and custom safety barriers, *Composite Structures*, 133 (2015), 659-666.
8.Manalo A and Jackson M. Behaviour of pultruded glass fibre reinforced composites guardrail system, *Advances in Structural Engineering*, 21(4) (2018), 545-556.
9.Manalo A and Pac M. Structural behaviour of pultruded fibre composites guardrail system under horizontal loading, *Proceedings of the Institution of Mechanical Engineers Part L, Journal of Materials: Design and Applications,* 232(4) (2018), 273-286.
10.Bank LC and Gentry TR Development of a pultruded composite material highway guardrail, *Composites – Part A: Applied Science and Manufacturing,* 32(9) (2001), 1329-1338.
11.BS 4592-0:2006+A1:2012, Flooring, stair treads and handrails for industrial use. Common design requirements and recommendations for installation. British Standards Institution, London, 2012.
12.BS EN ISO 144122-3: 2013, Safety of machinery – permanent means of access to machinery part 3: Stairs, stepladders and guard-rails. British Standards Institution, London, 2013.

List of Figures and Captions

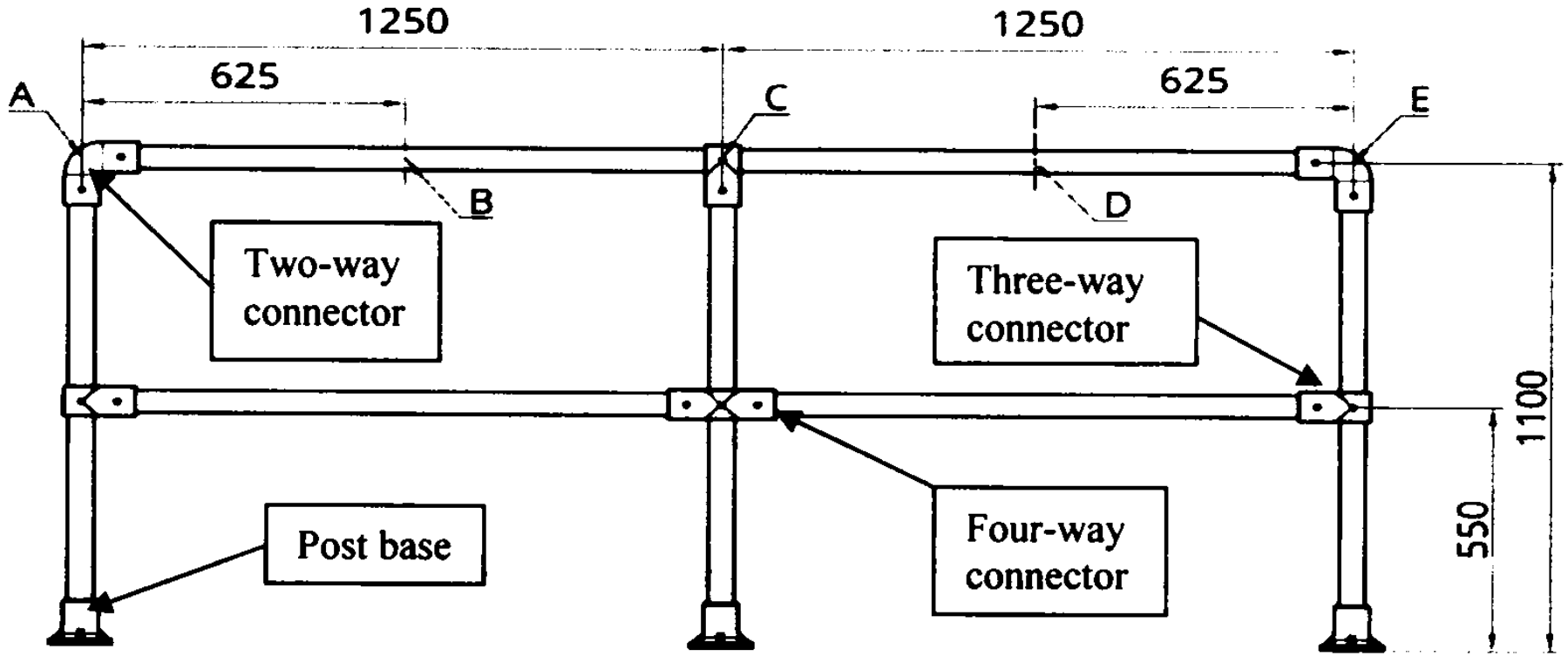
1250
1250
625
625
A
B
C
D
E
Two-way connector
Three-way connector
Post base
Four-way connector
1100
550

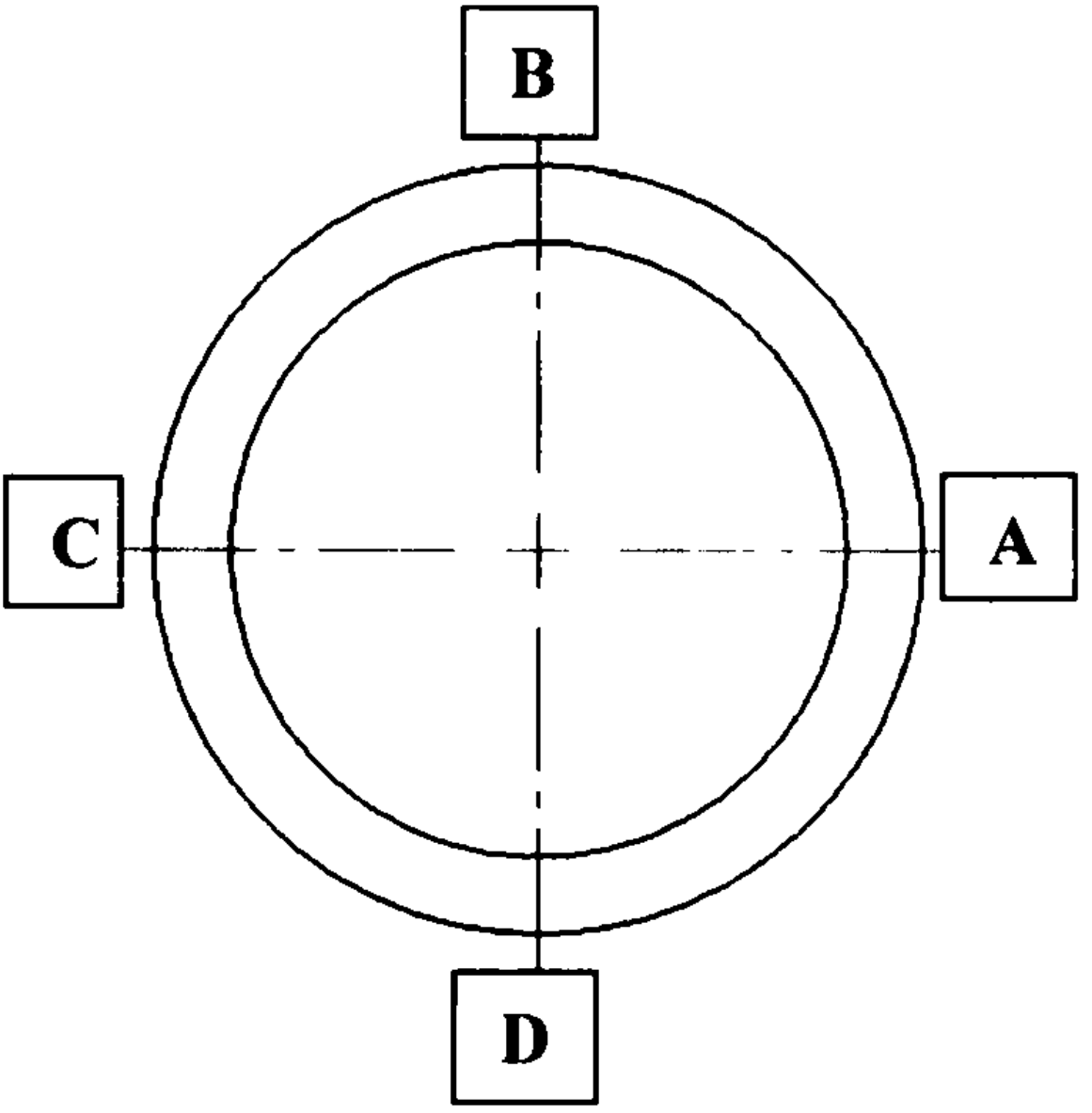
B
C
A
D

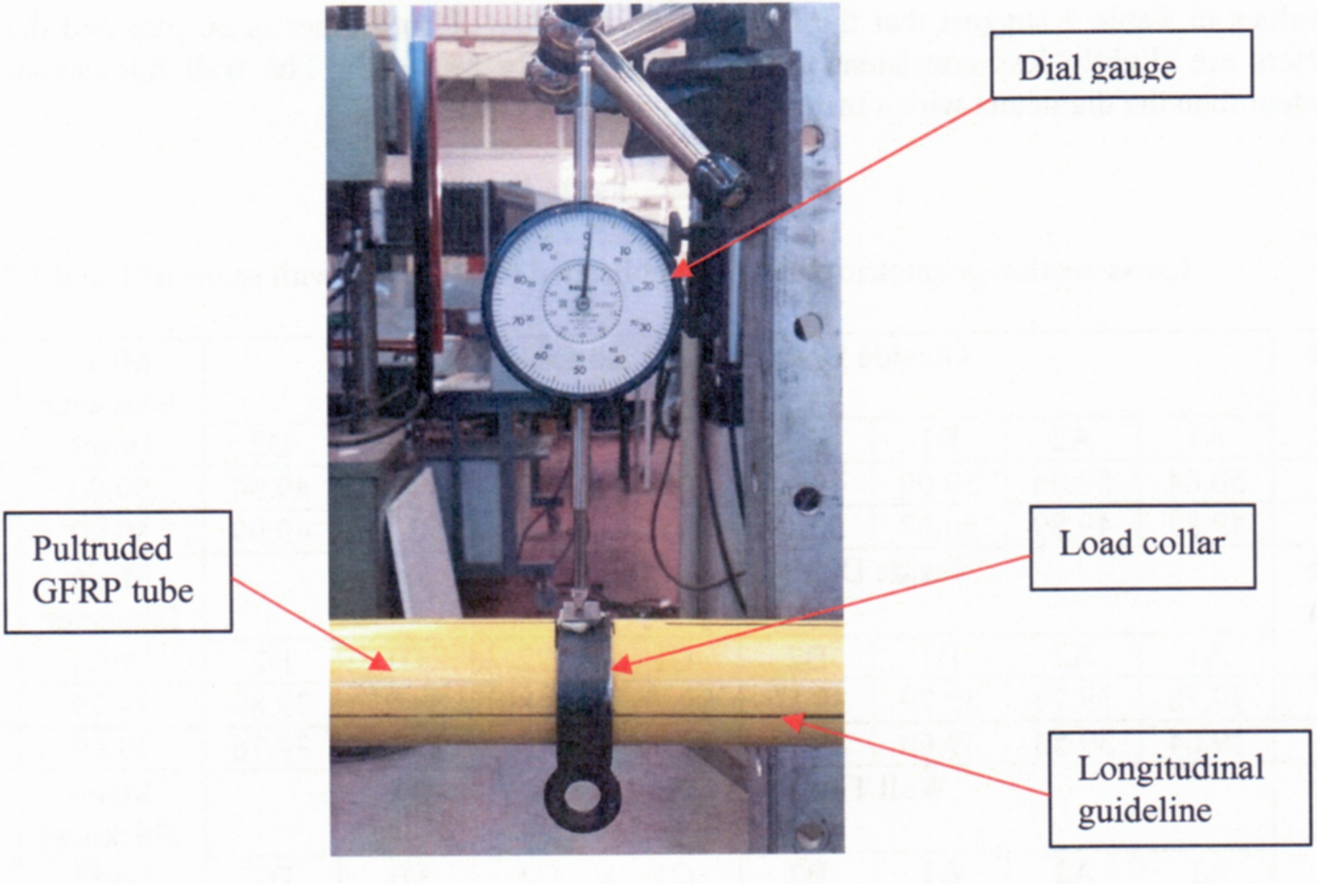
Dial gauge
Pultruded GFRP tube
Load collar
Longitudinal guideline

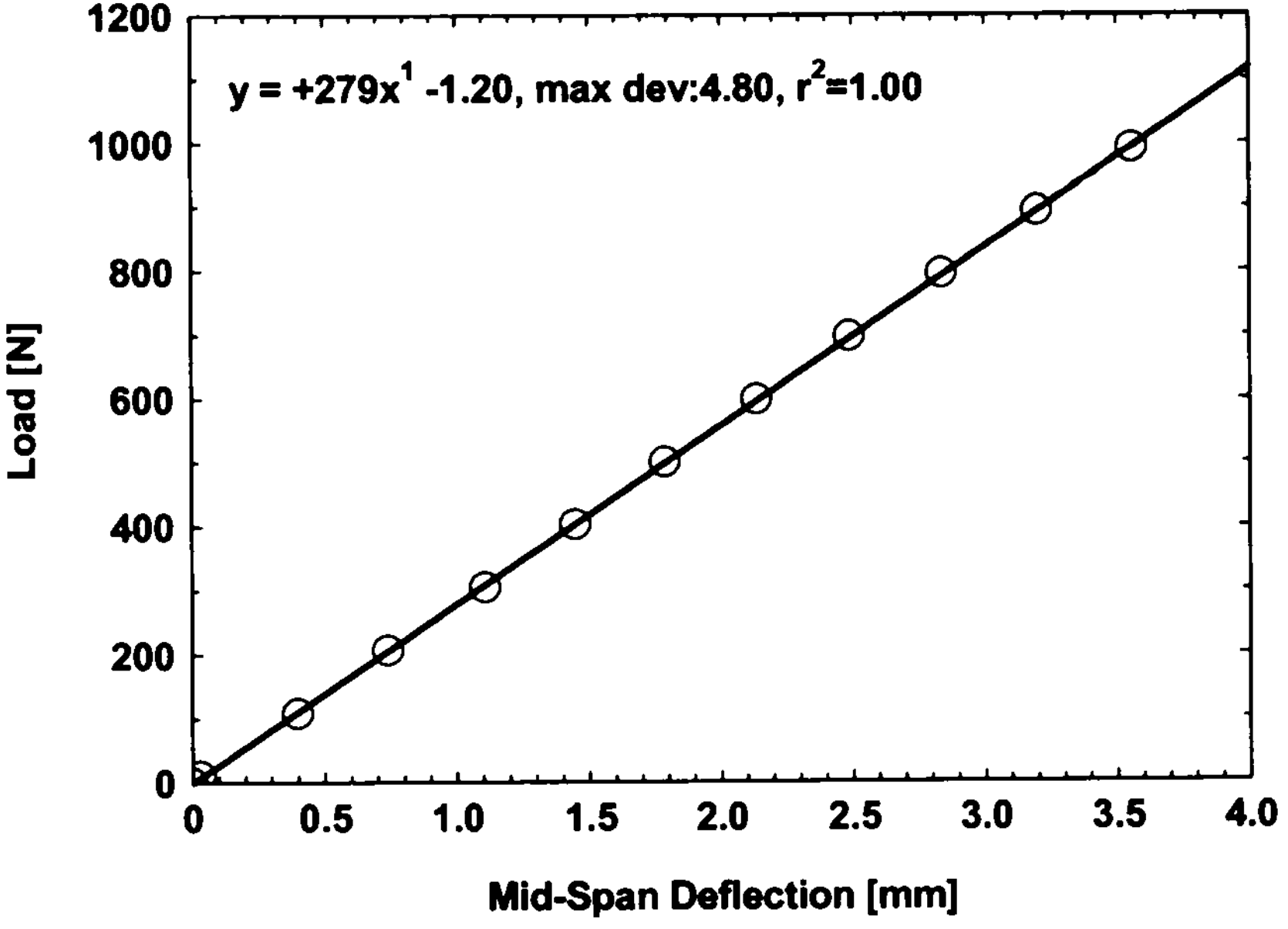
y = +279x^1 -1.20, max dev:4.80, r^2=1.00
Load [N]
Mid-Span Deflection [mm]
0
200
400
600
800
1000
1200
0
0.5
1.0
1.5
2.0
2.5
3.0
3.5
4.0

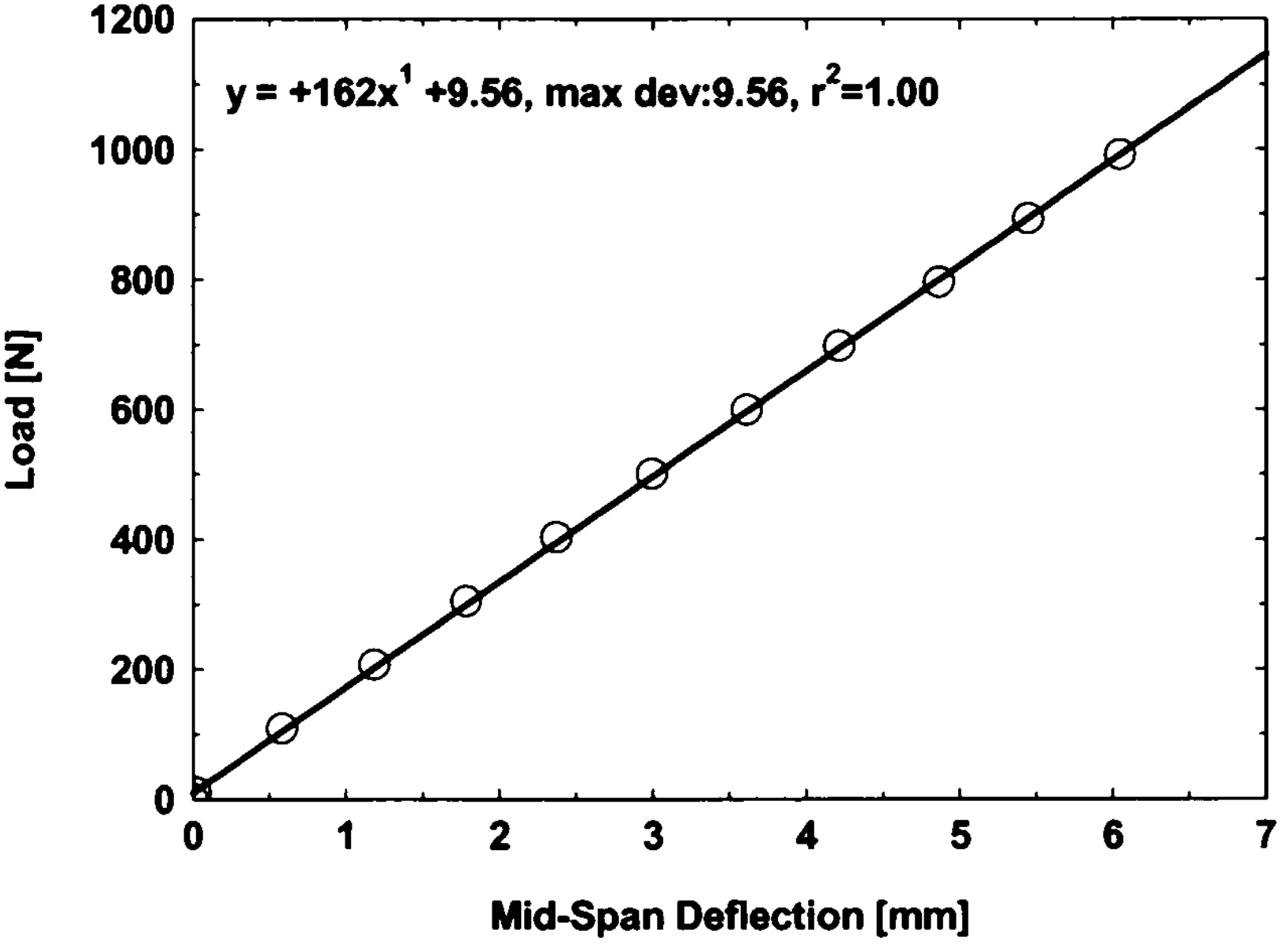
y = +162x^1 +9.56, max dev:9.56, r^2=1.00
Load [N]
Mid-Span Deflection [mm]
0
200
400
600
800
1000
1200
0
1
2
3
4
5
6
7

(b)

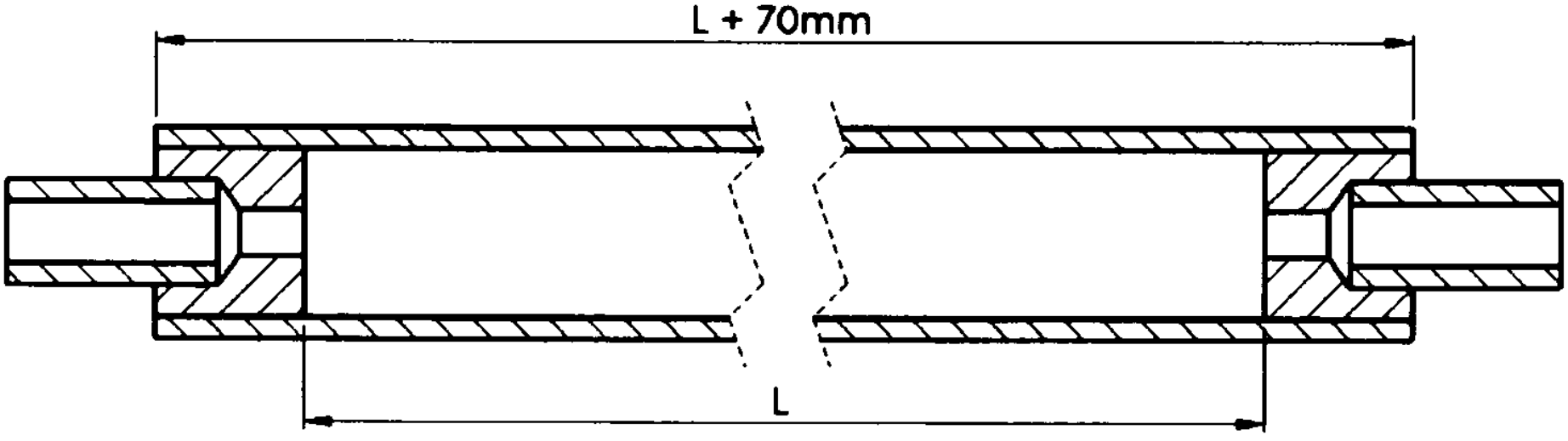
L + 70mm
L

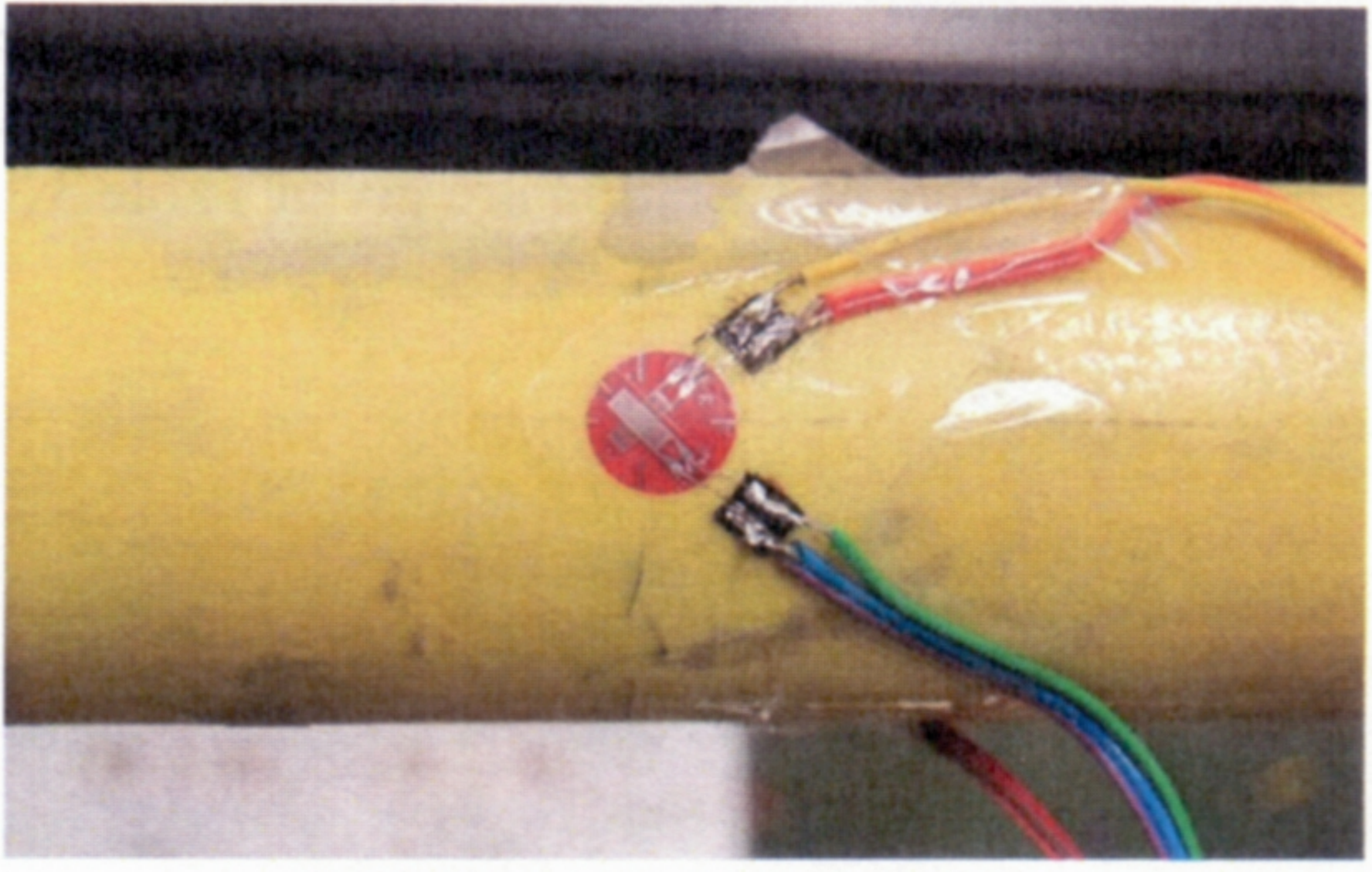

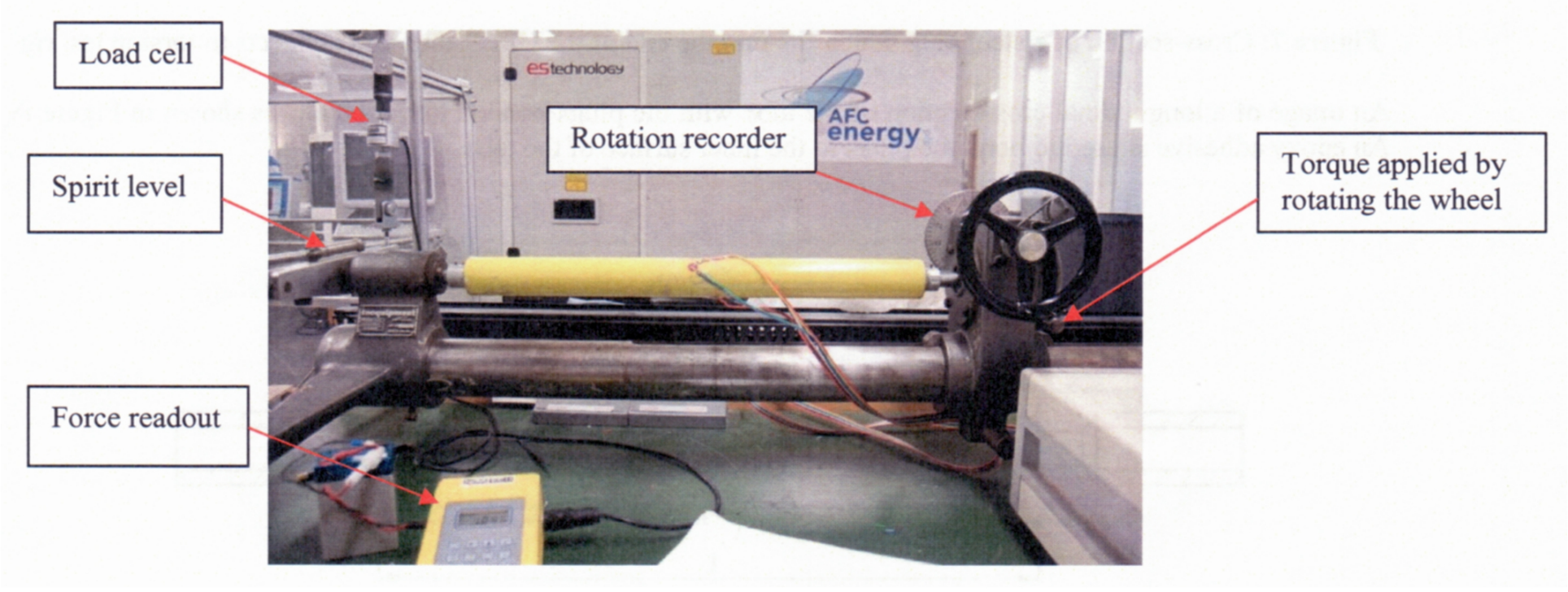
Load cell
Spirit level
Force readout
Rotation recorder
Torque applied by rotating the wheel
esTechnology
AFC energy

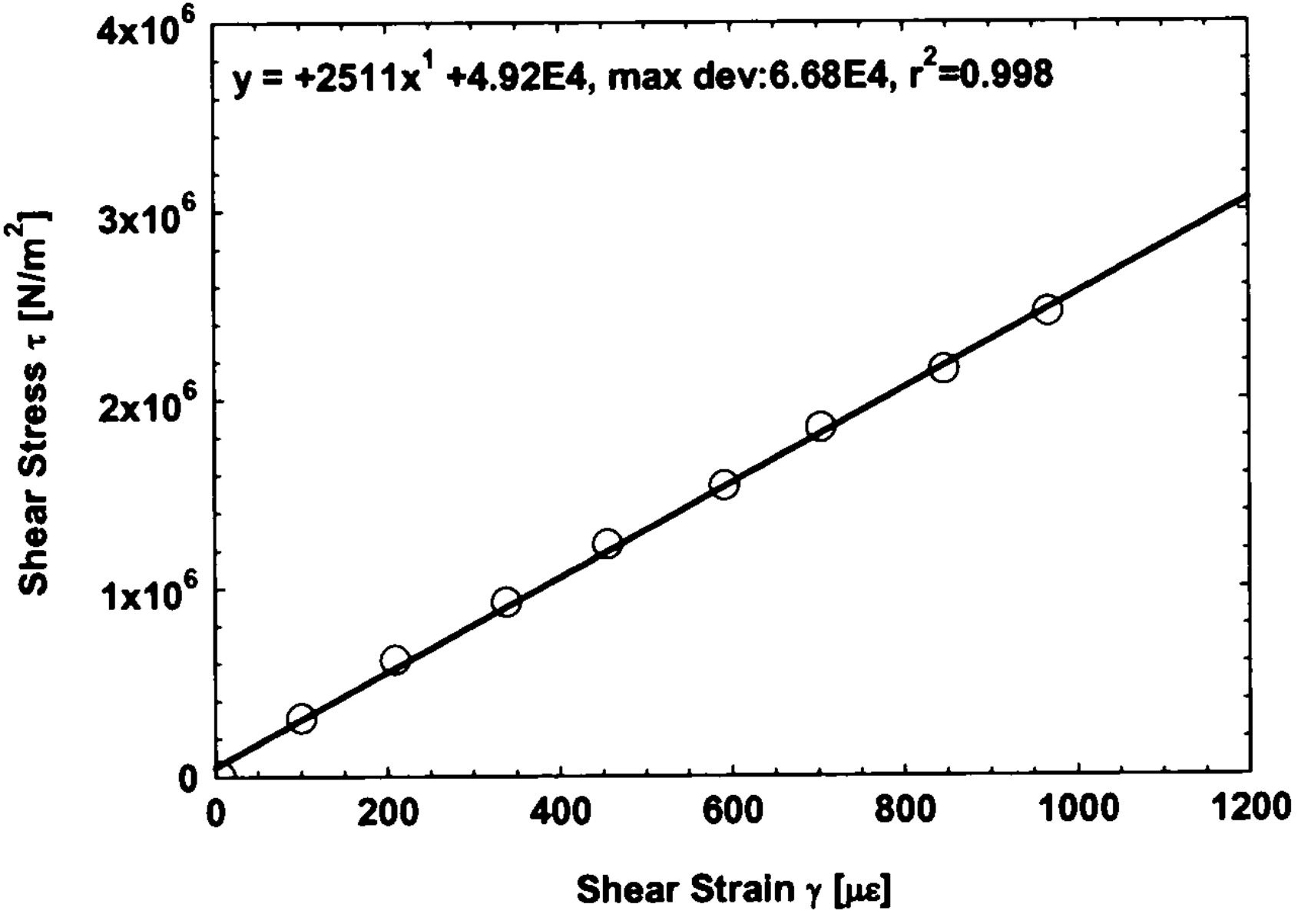
y = +2511x^1 +4.92E4, max dev:6.68E4, r^2=0.998
Shear Stress τ [N/m^2]
Shear Strain γ [με]
4x10^6
3x10^6
2x10^6
1x10^6
0
0
200
400
600
800
1000
1200

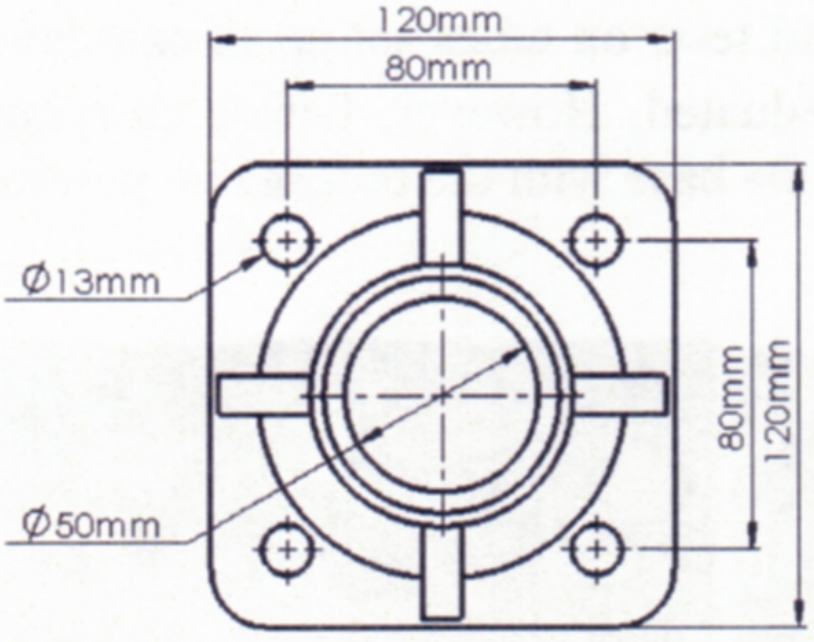
120mm
80mm
Ø13mm
Ø50mm
80mm
120mm

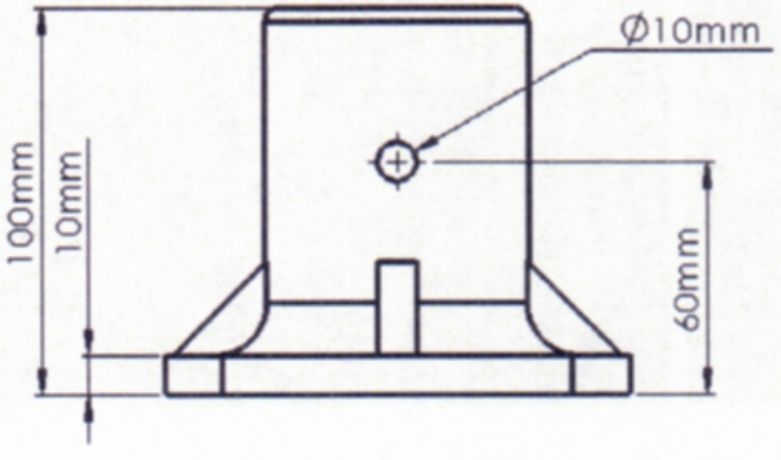
Ø10mm
100mm
10mm
60mm

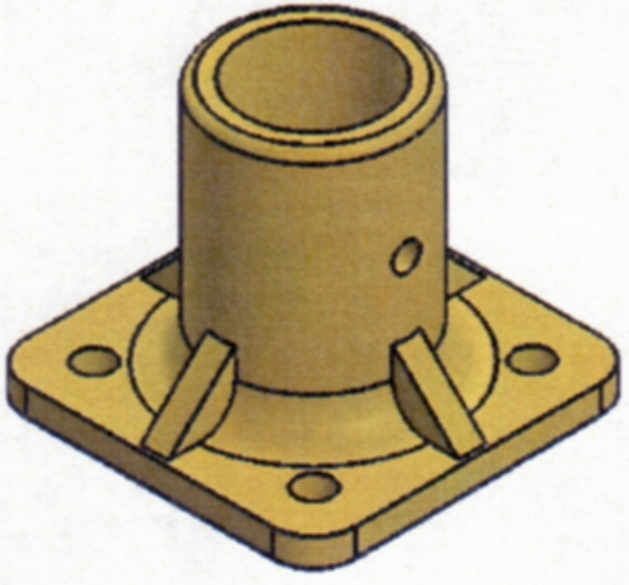

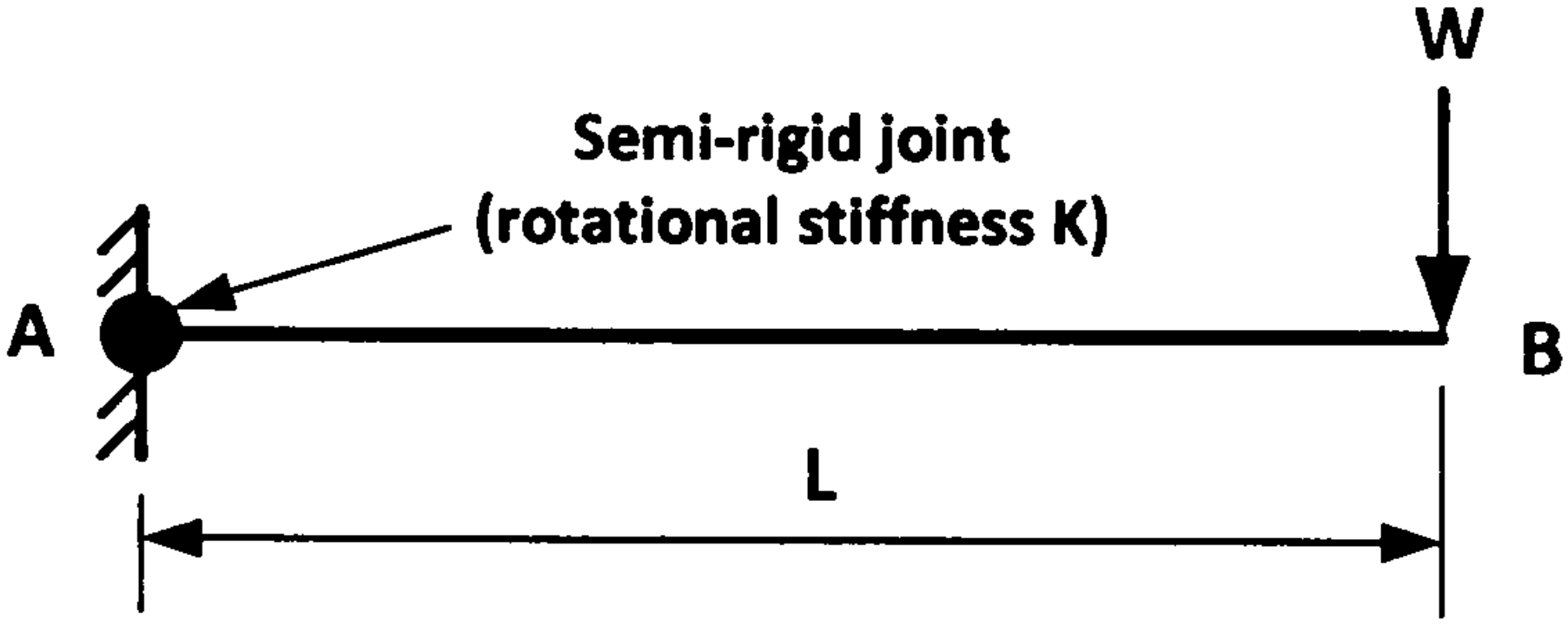
W
Semi-rigid joint
(rotational stiffness K)
A
B
L

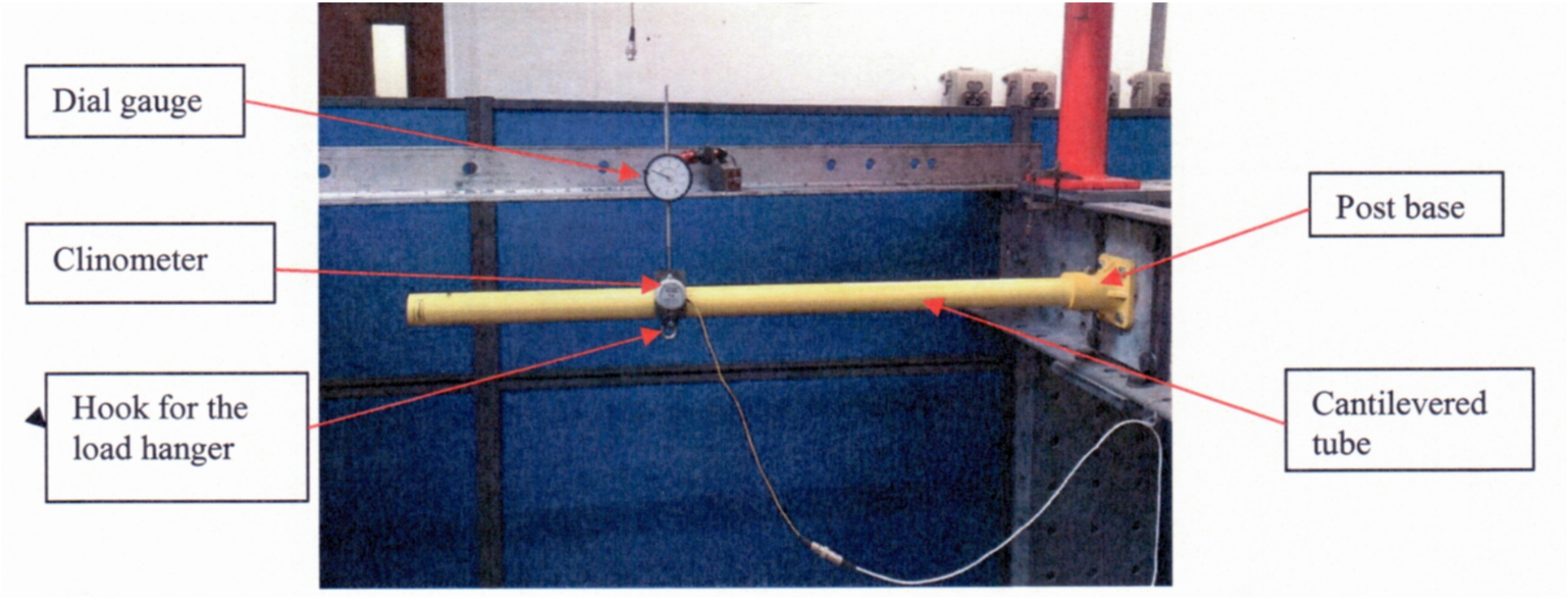
Dial gauge
Clinometer
Hook for the load hanger
Post base
Cantilevered tube

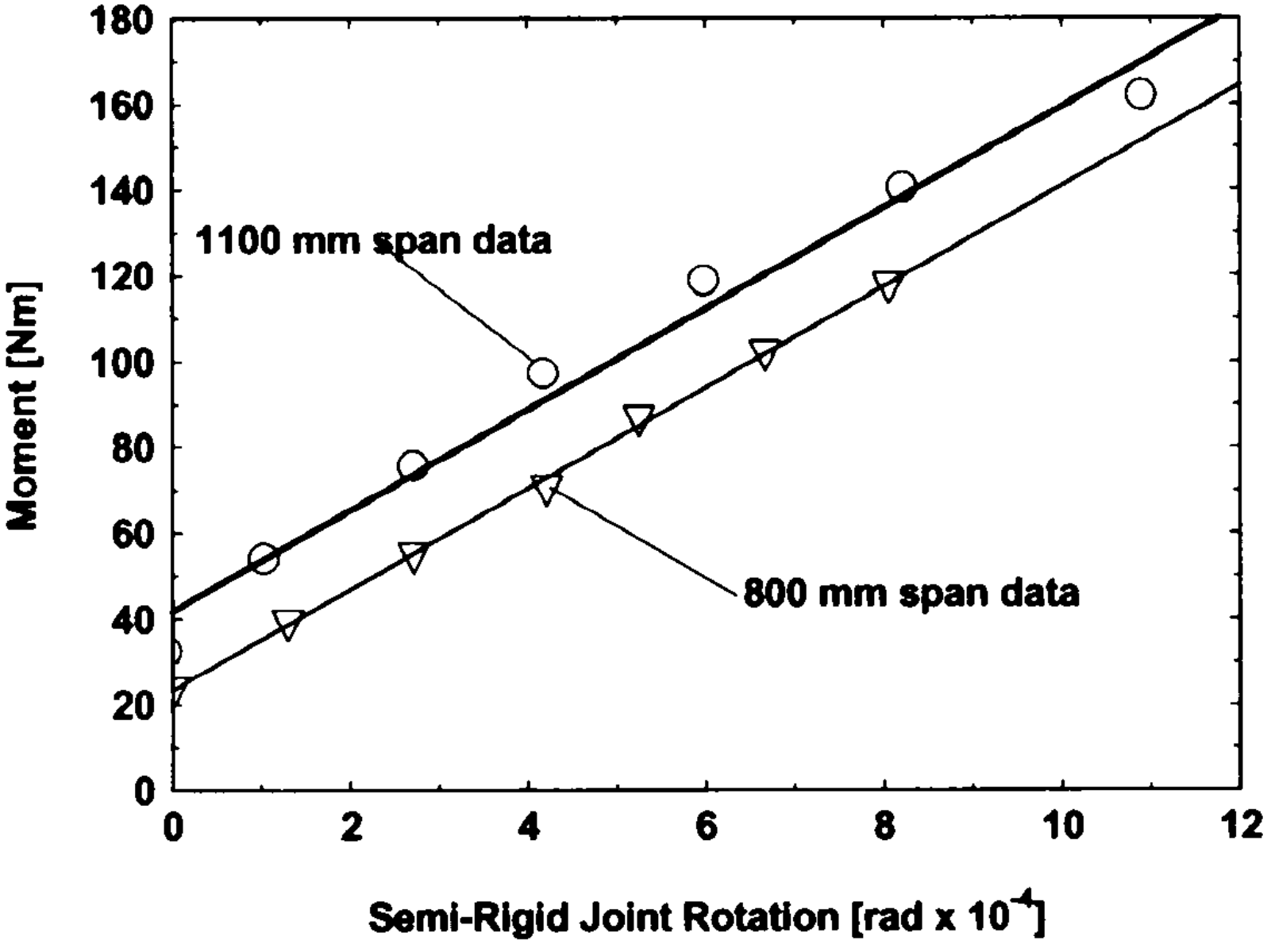
180
160
140
120
100
80
60
40
20
0
Moment [Nm]
1100 mm span data
800 mm span data
0
2
4
6
8
10
12
Semi-Rigid Joint Rotation [rad x 10-4]

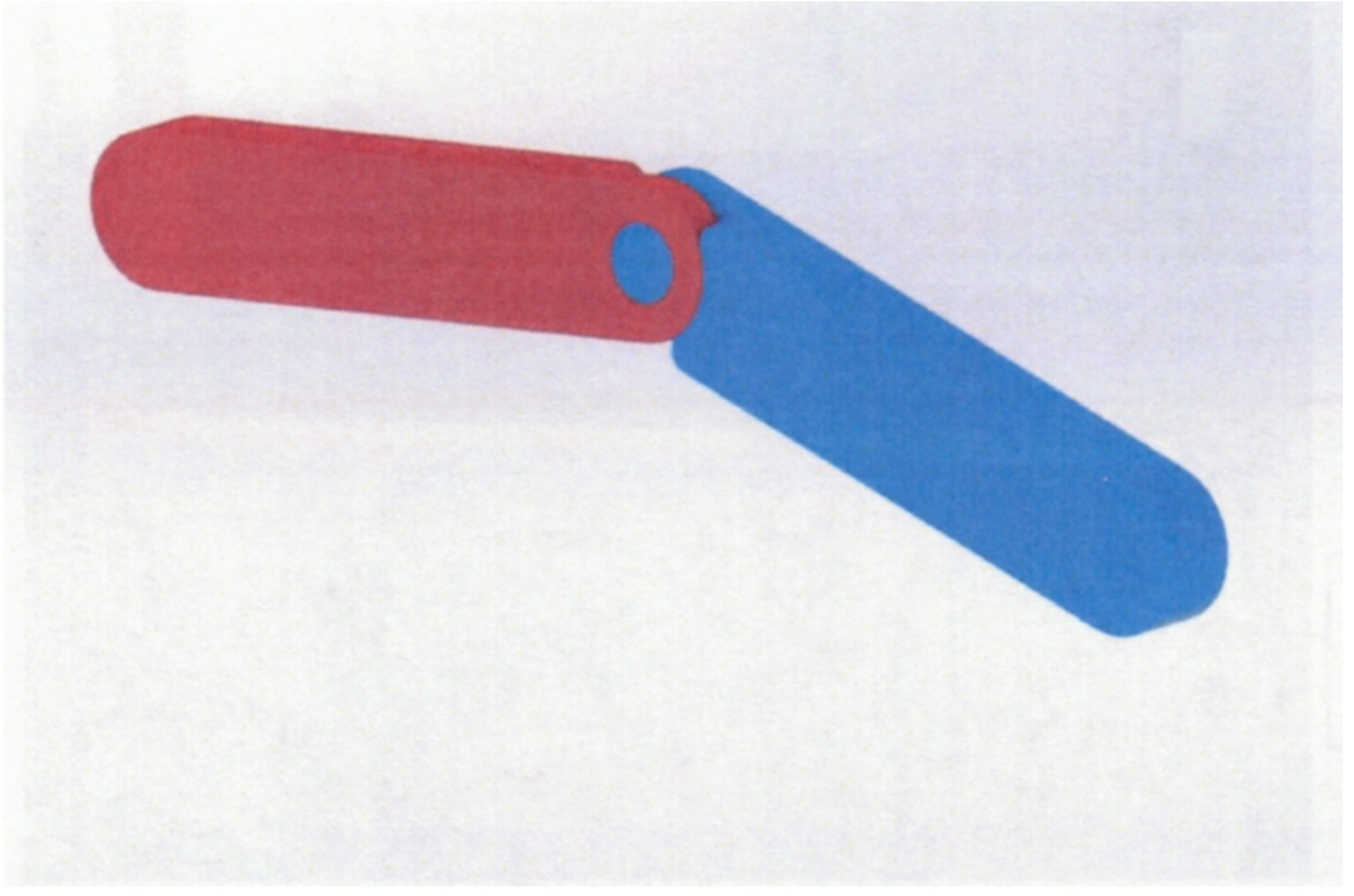

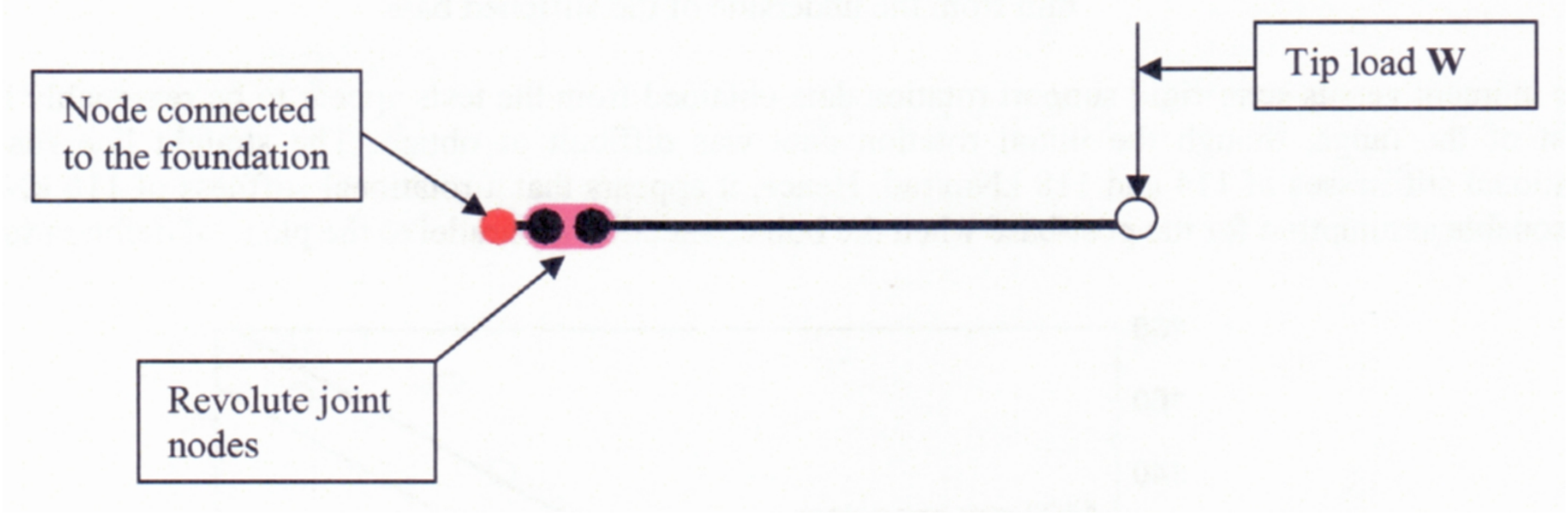
Node connected to the foundation
Tip load **W**
Revolute joint nodes

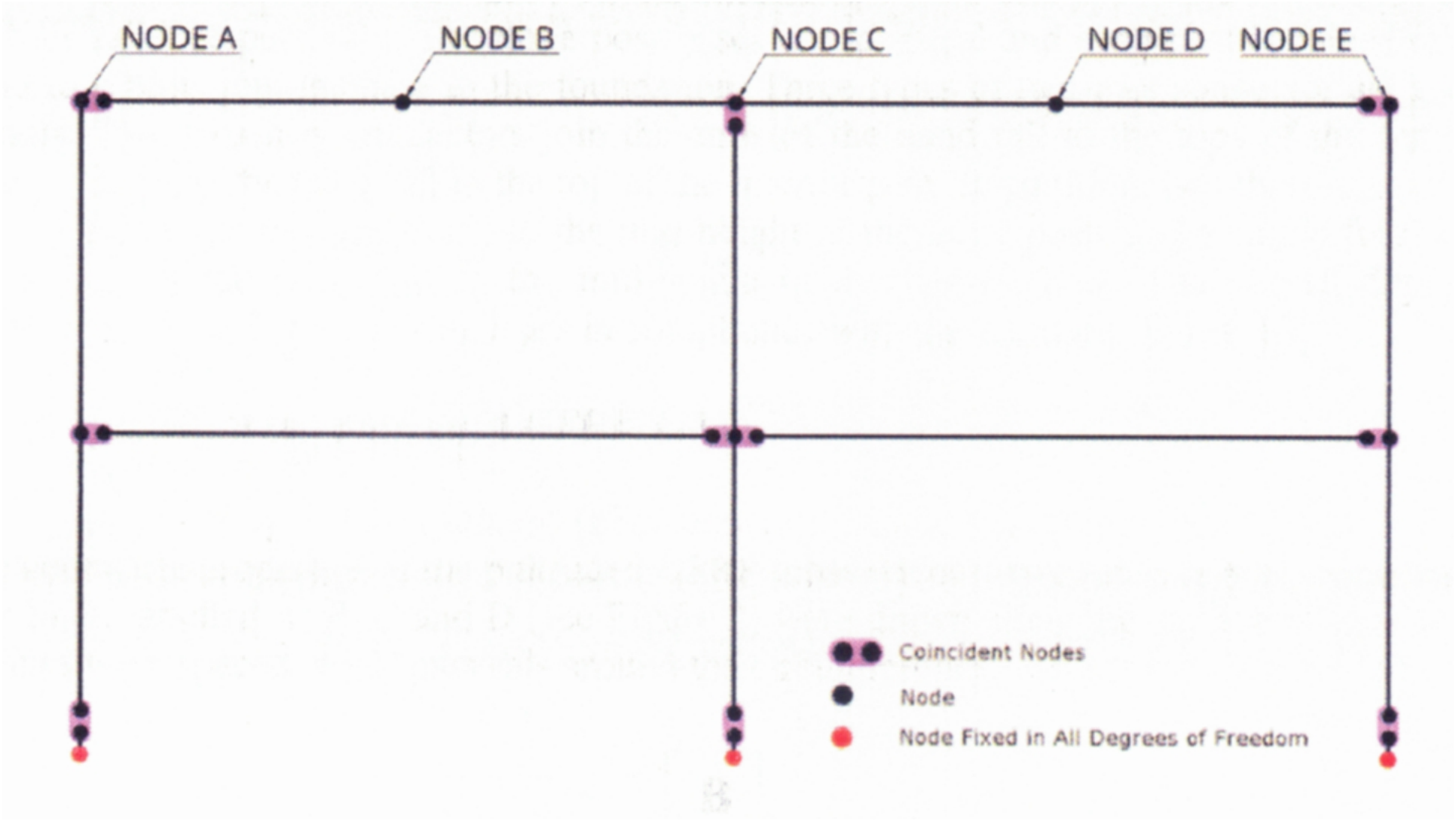
NODE A
NODE B
NODE C
NODE D
NODE E
Coincident Nodes
Node
Node Fixed in All Degrees of Freedom

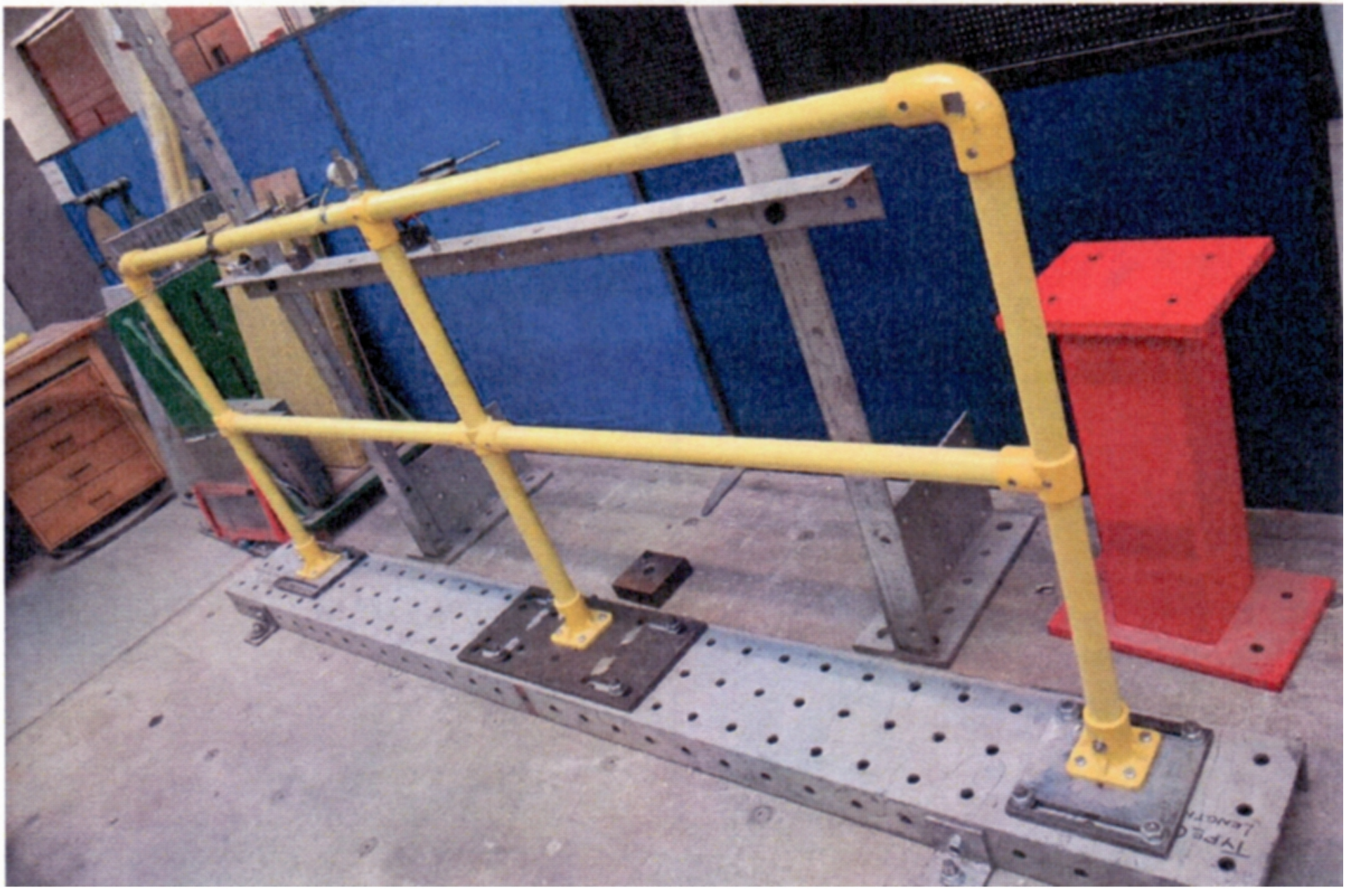

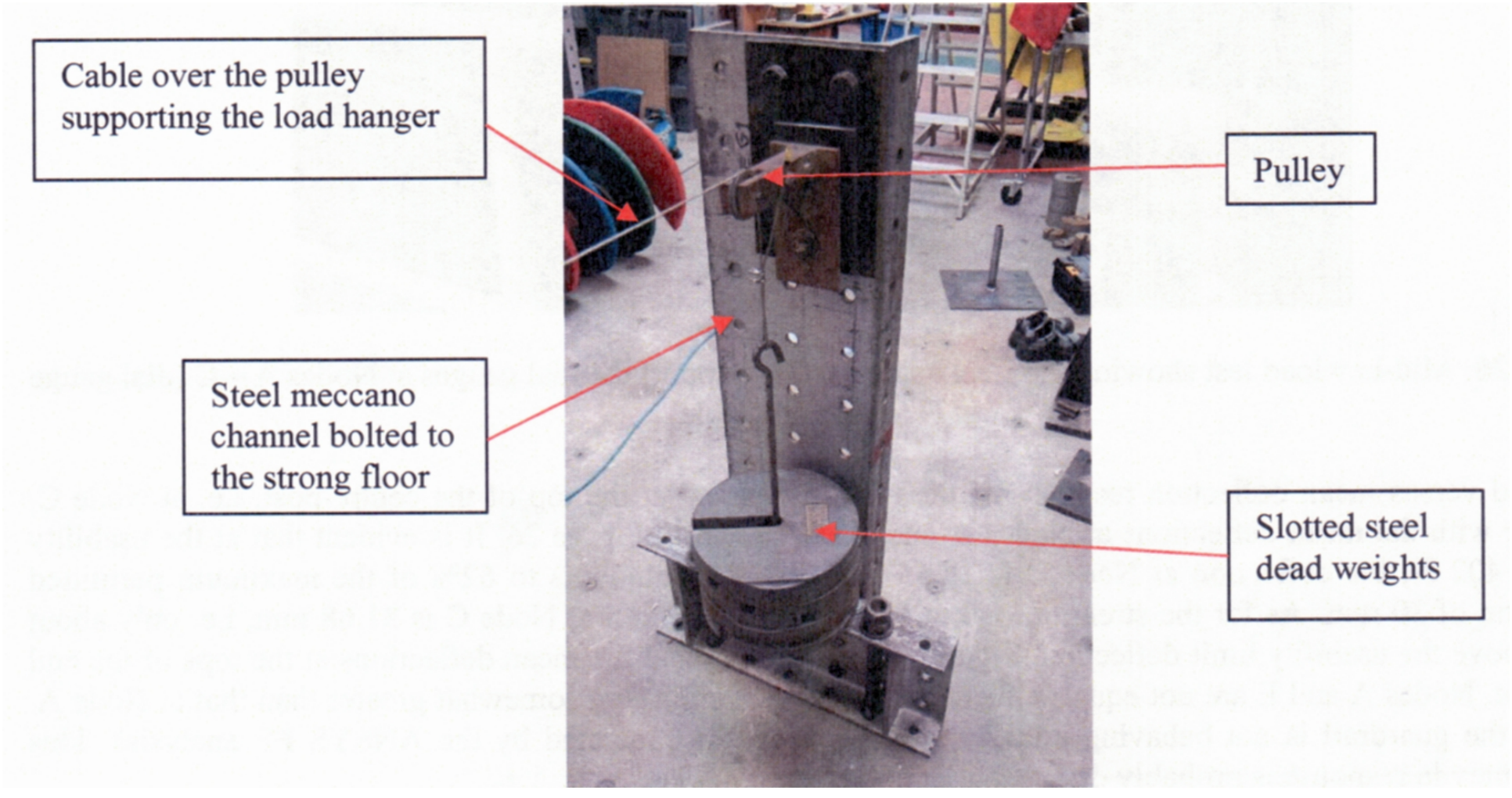
Cable over the pulley supporting the load hanger
Pulley
Steel meccano channel bolted to the strong floor
Slotted steel dead weights

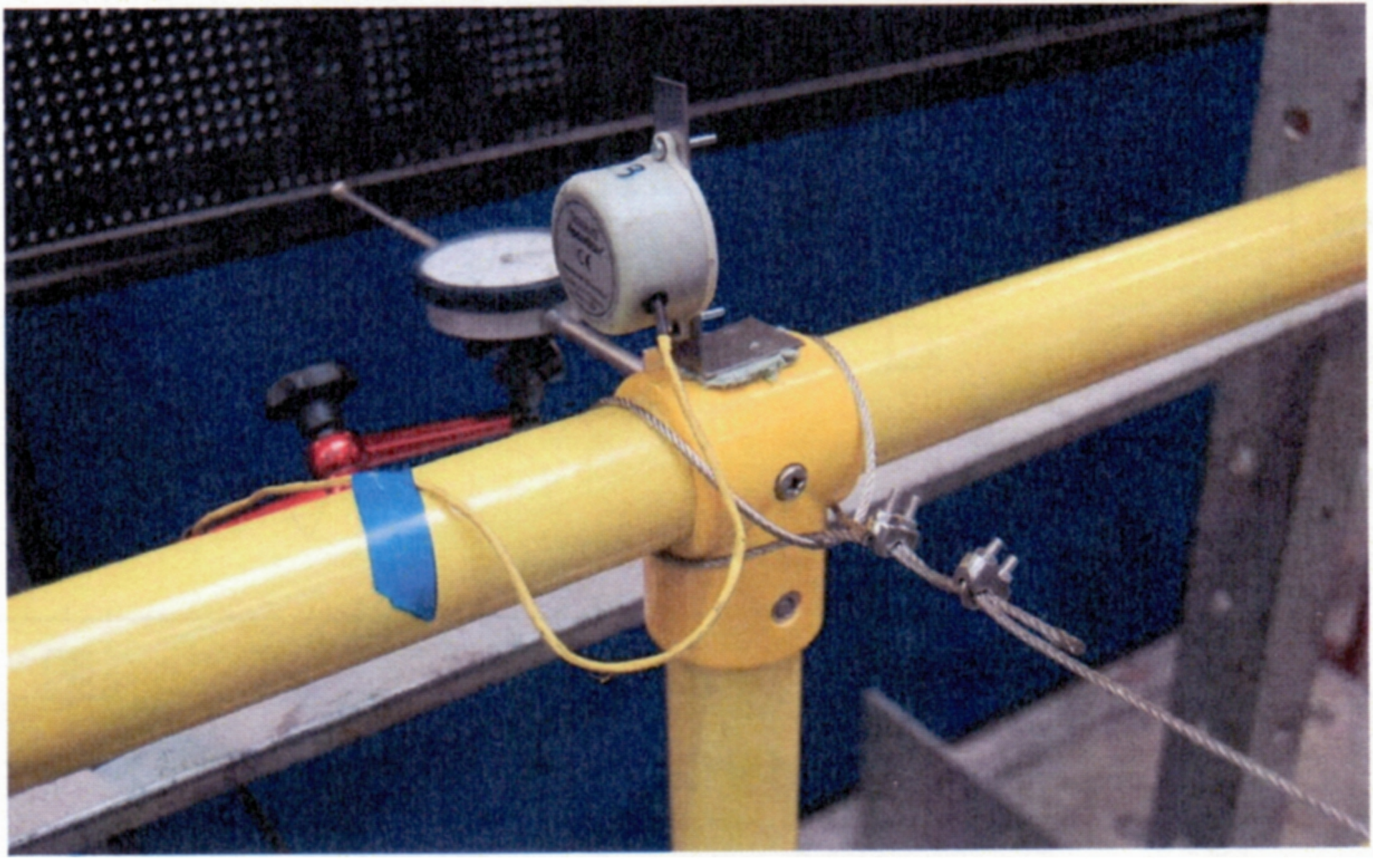

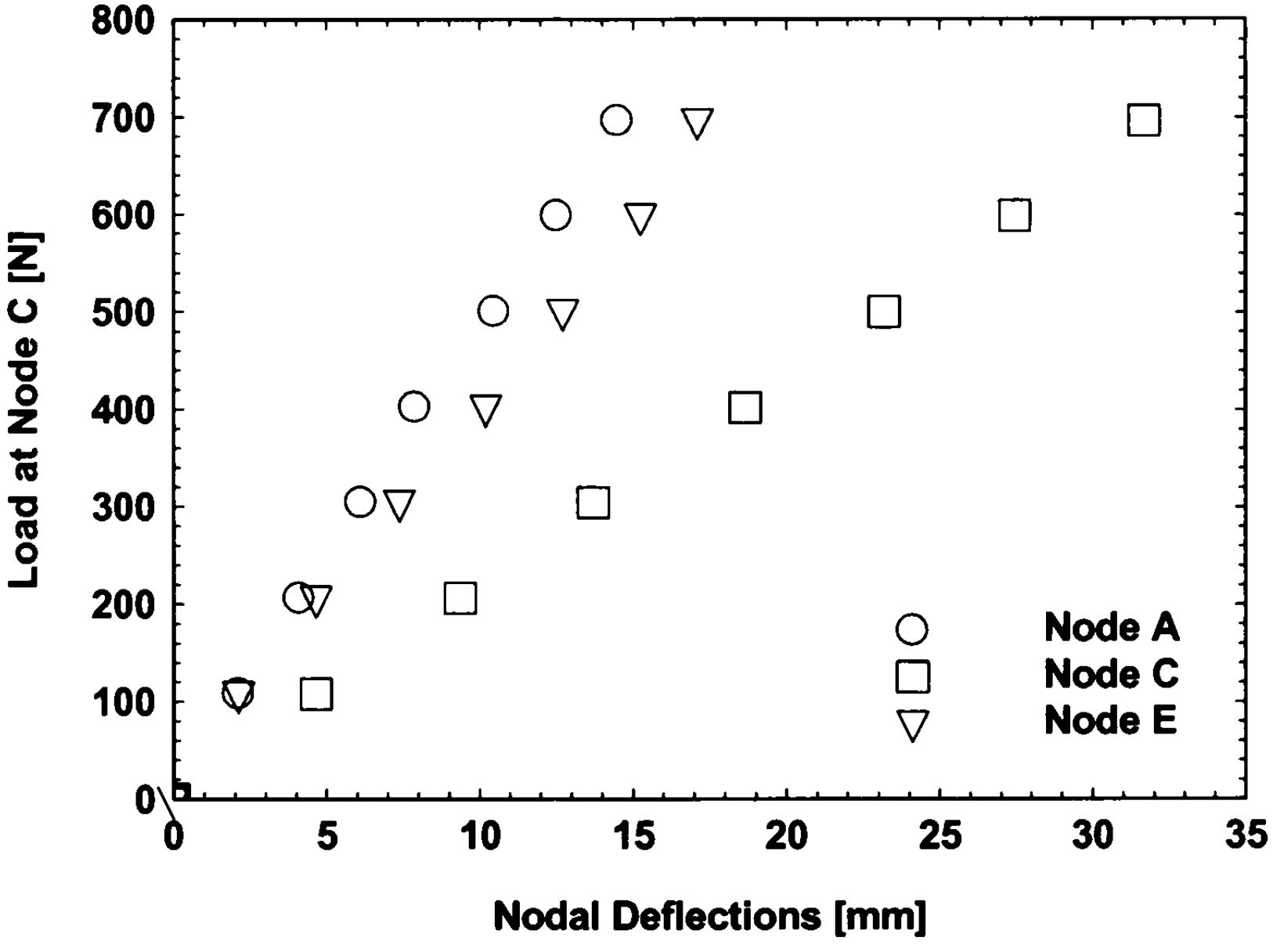
800
700
600
500
400
300
200
100
0
Load at Node C [N]
0
5
10
15
20
25
30
35
Nodal Deflections [mm]
Node A
Node C
Node E

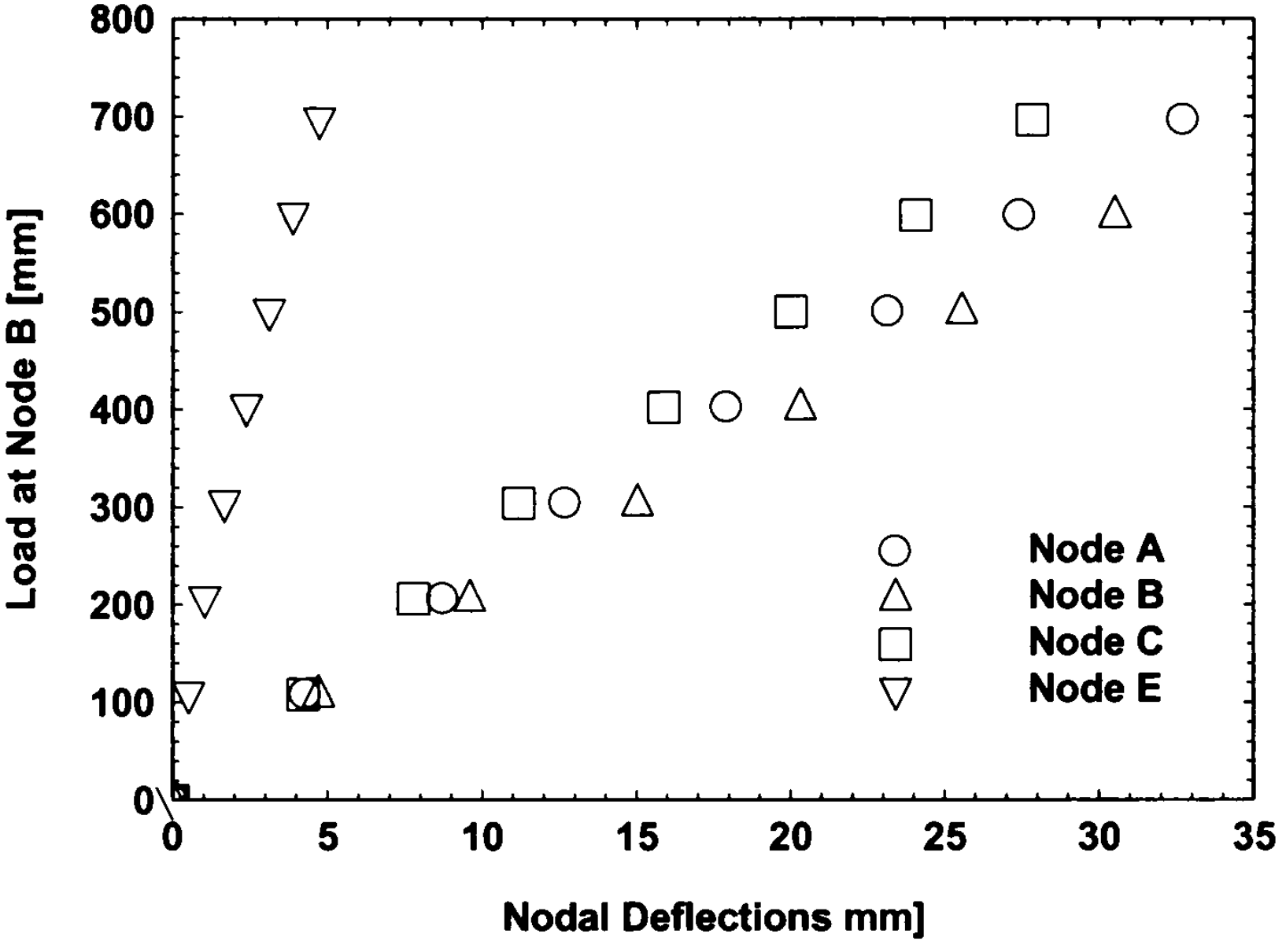
800
700
600
500
400
300
200
100
0
Load at Node B [mm]
0
5
10
15
20
25
30
35
Nodal Deflections mm]
Node A
Node B
Node C
Node E

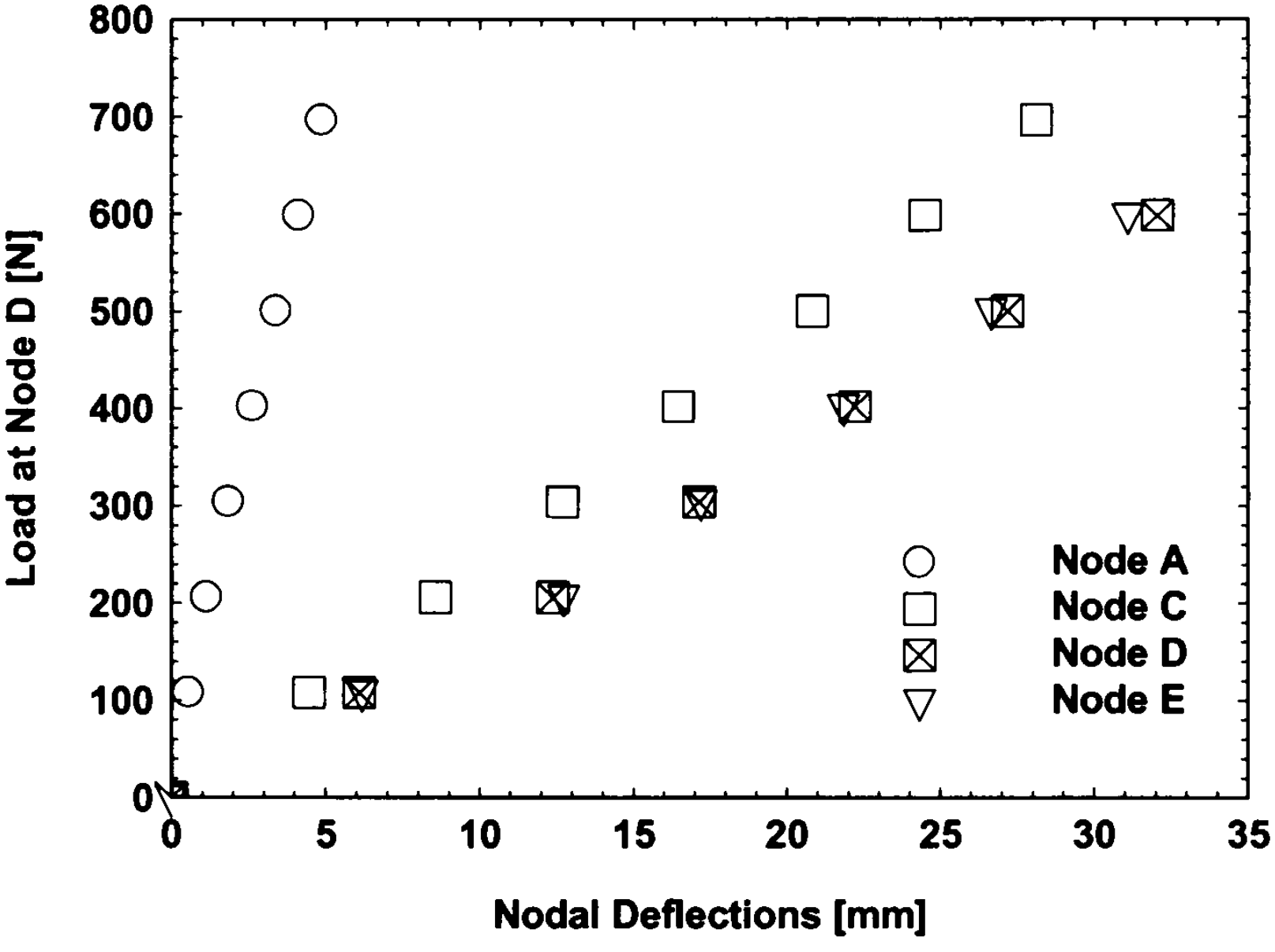
800
700
600
500
400
300
200
100
0
Load at Node D [N]
0
5
10
15
20
25
30
35
Nodal Deflections [mm]
Node A
Node C
Node D
Node E

Table 1

Cross-section geometric data for the pultruded GFRP tubes with spans of 1 and 1.2 m

Tube Length	Outside Diameters at Line Ends [mm]								Mean Diameter	S.D.	C.V.
[m]	A1	A2	B1	B2	C1	C2	D1	D2	[mm]	[mm]	[mm]
1.0	50.04	50.06	50.00	49.95	50.07	49.95	50.01	49.94	50.00	0.048	0.001
1.2	49.87	49.89	50.02	50.10	50.02	49.99	50.13	49.99	50.00	0.084	0.002
Tube Length	Inside Diameters at Line Ends [mm]								Mean Diameter	S.D.	C.V.
[m]	A1	A2	B1	B2	C1	C2	D1	D2	[mm]	[mm]	[mm]
1.0	39.78	39.74	39.79	39.80	39.76	39.80	39.87	39.80	39.79	0.036	0.001
1.2	39.64	39.53	39.69	39.76	39.75	39.67	39.69	39.76	39.69	0.072	0.002
Tube Length	Wall Thickness at Line Ends [mm]								Mean Thickness	S.D.	C.V.
[m]	A1	A2	B1	B2	C1	C2	D1	D2	[mm]	[mm]	[mm]
1.0	5.06	4.95	5.09	5.06	5.29	5.21	5.01	5.12	5.10	0.102	0.020
1.2	5.11	5.01	5.26	5.20	5.16	5.11	5.12	4.93	5.11	0.097	0.019

Notes: A1, A2 etc. denote location A at tube ends 1 and 2, respectively. S.D. denotes Standard Deviation and C.V. denotes Coefficient of Variation

Table 2

Flexural elastic moduli derived from the load versus mean mid-span deflection tests for the four orientations (A – D) of the 1 and 1.2 m span simply supported tube tests

Span (L) [m]	**Second Moment of Area (I)** [$mm^4 x\ 10^{-9}$]	**Load (W)** [N]	**Mid-Span Deflection (d)** [mm]	**Elastic Flexural Modulus (E)** [GPa]
1	183.75	559	2	31.69
		557		31.58
		580		32.88
		561		31.80
1.2	184.98	658	4	32.01
		680		33.08
		649		31.58
		672		32.70
Mean Elastic Flexural Modulus				**32.17**
Standard Deviation of Flexural Modulus				**0.58**

Table 3

Cross-section geometric data of the pultruded GFRP tubes with torsion spans of 0.3, 0.4 and 0.5 m

Location	**Outside Diameter Measurements**			
	Diameter [mm]	**Mean [mm]**	**S.D. [mm]**	**C.V.**
A	49.83	49.98	0.106	0.002
B	50.04			
C	49.94			
D	50.11			
	Inside Diameter Measurements			
Location	**Diameter [mm]**	**Mean [mm]**	**S.D. [mm]**	**C.V.**
A	39.70	39.72	0.109	0.003
B	39.55			
C	39.81			
D	39.82			
	Wall Thickness Measurements			
Location	**Wall Thickness [mm]**	**Mean [mm]**	**S.D. [mm]**	**C.V.**
A	5.14	5.185	0.197	0.038
B	5.49			
C	5.17			
D	4.94			

Table 4

Individual shear and mean shear moduli and standard deviation

Tube Length [mm]	τ [Nm^{-2} x 10^6]	γ [x 10^3]	G [GPa]
300	1.51	600	2.52
400	1.51	600	2.52
500	1.48	600	2.47
Mean Shear Modulus			2.50
Standard Deviation of Shear Modulus			0.024

Table 5

Cross-section geometric data of the pultruded GFRP tubes with spans of 1.1 and 0.8 m used in the tests on cantilevers with semi-rigid end connections

Tube Span [m]	Outside Diameters at Line Ends [mm]								Mean Diameter [mm]	S.D. [mm]	C.V.
	A1	A2	B1	B2	C1	C2	D1	D2			
1.1, 0.8	49.83	49.88	50.04	49.97	49.94	50.05	50.11	50.21	50.00	0.116	0.002
Tube Span [m]	Inside Diameters at Line Ends [mm]								Mean Diameter [mm]	S.D. [mm]	C.V. [mm]
	A1	A2	B1	B2	C1	C2	D1	D2			
1.1, 0.8	39.70	39.62	39.55	39.34	39.81	39.63	39.82	39.70	39.65	0.144	0.004
Tube Span [m]	Wall Thickness at Line Ends [mm]								Mean Thickness [mm]	S.D. [mm]	C.V. [mm]
	A1	A2	B1	B2	C1	C2	D1	D2			
1.1, 0.8	5.14	5.07	5.49	4.97	5.17	5.19	4.94	5.34	5.16	0.172	0.033

Notes: A1, A2 etc. denote location A at tube ends 1 and 2, respectively. S.D. denotes Standard Deviation and C.V. denotes Coefficient of Variation

Table 6

Comparison of FE and experimental tip deflections and rotations of semi-rigid cantilevers

[Tube Data: Inner and Outer Diameters = 20 & 25 mm; Flexural and Shear Moduli = 32.17 & 2.5 GPa; Poisson's Ratio = 0.33; Semi-Rigid Joint Stiffness = 116 Nm/rad]

Tip Load (W) [N]	**Mean Exp. Tip Deflection (δ_B)** [mm]	**Mean Exp. Tip Rotation (θ_B)** [mrad]	**ANSYS Tip Deflection (δ_B)** [mm]	**ANSYS Tip Rotation (θ_B)** [mrad]
800 mm Span				
29.43	0.85	1.59	1.06	1.83
49.05	1.51	3.03	1.76	3.05
68.67	2.18	4.33	2.46	4.27
88.29	2.87	5.41	3.17	5.47
107.91	3.51	6.58	3.87	6.71
127.53	4.19	7.72	4.58	7.93
147.15	4.86	0.00890	5.28	9.14
1100 mm Span				
29.43	2.12	3.63	2.60	3.35
49.05	3.76	6.04	4.33	5.59
68.67	5.41	8.05	6.06	7.82
88.29	7.03	10.16	7.79	10.06
107.91	8.69	12.24	9.52	12.29
127.53	10.39	14.39	11.26	14.53
147.15	12.15	16.57	12.99	16.76

Table 7

Nodal deflections normal to the plane of the guardrail with the maximum load applied at Node C

Model Number	Node A Deflection [mm]	Node B Deflection [mm]	Node C Deflection [mm]	Node D Deflection [mm]	Node E Deflection [mm]
	Load of 697 N applied at Node C				
1	12.40	21.24	25.50	21.24	12.40
2	14.57	23.70	28.10	23.70	14.57
3	14.56	23.71	28.11	23.71	14.56
	Load of 697 N applied at Node B				
1	25.00	27.87	21.24	12.57	4.06
2	28.50	30.90	23.70	14.32	5.03
3	28.50	30.90	23.70	14.32	5.03

Table 8

Calculated and actual loads used in the two-bay guardrail tests

Bay Span [m]	**Type of Test**	**Calculated Load [N]**	**Actual Load [N]**	**Maximum Deflection [mm]**	**Residual Deflection after Unloading [mm]**
1.25	F_p	93.75	108	-	-
	F_u	375	402	< 30	
	F_s	656.25	697		3.75

Table 9

Comparison of the deflections of FE Models 1 – 3 with average test values for centre-post loading of 697N

Model/Test	**Deflection at Node A [mm]**	**Deflection at Node B [mm]**	**Deflection at Node C [mm]**	**Deflection at Node D [mm]**	**Deflection at Node E [mm]**
1	12.40	21.24	25.50	21.24	12.40
2	14.57	23.70	28.10	23.70	14.57
3	14.56	23.71	28.11	23.71	14.56
Test	**14.50**	**-**	**31.68**	**-**	**17.11**

Table 10

Comparison of the deflections of FE Models 1 – 3 with average test values for the two cases of mid bay loading

Model/Test	**Deflection at Node A [mm]**	**Deflection at Node B [mm]**	**Deflection at Node C [mm]**	**Deflection at Node D [mm]**	**Deflection at Node E [mm]**
	Load of 697 N applied at Node B				
1	25.00	27.87	21.24	12.57	4.06
2	28.50	30.90	23.70	14.32	5.03
3	28.50	30.90	23.70	14.32	5.03
Test*	**32.71**	**35.56**	**27.83**		**4.75**
	Load of 697 N applied at Node D				
1	4.06	12.57	21.24	27.87	25.00
2	5.03	14.32	23.70	30.90	28.50
3	5.03	14.32	23.70	30.90	28.50
Test*	**4.88**		**28.12**	**36.84**	**35.46**

*The values in the row are the mean deflections of three repeat tests with the load applied at the relevant node

Conflict of Interests Form

The Authors certify that they have no conflict of interests.

Please note: The Authors could not locate a Conflict of Interests Form on the website for the Composite Structures Journal, so they have uploaded this Word File instead.

Declaration of interests

 The authors declare that they have no known competing financial interests or personal relationships that could have appeared to influence the work reported in this paper.

☐The authors declare the following financial interests/personal relationships which may be considered as potential competing interests: